Structure and dynamics of the upper atmospheres of Venus and Mars

M. N. Izakov

Institute of Cosmic Research, USSR Academy of Sciences
Usp. Fiz. Nauk 119, 295–342 (June 1976)

PACS numbers: 96.40.Fg, 96.40.Gh

CONTENTS

1. INTRODUCTION

The upper atmosphere of a planet is regarded as the region of the atmosphere whose structure and dynamics (temperature and density distribution, composition, and winds) are governed by the direct absorption of solar radiation. The diversity and complexity of the processes taking place in the upper atmospheres have made it necessary to develop their study into a separate branch of geophysics and astrophysics—aeronomy, which uses almost all branches of physics and some branches of chemistry.

Study of upper atmospheres has both practical and theoretical interest. Knowledge of the characteristics of the charged components of the upper atmosphere (which constitutes the ionosphere of the planet) is needed to improve radio communications and radio navigation (including space navigation); knowledge of the characteristics of the neutral upper atmosphere is needed to determine the trajectories and lifetimes of artificial satellites of the planets and the trajectories of space probes that enter the atmosphere. Clarification of the mechanisms by which the influence of solar activity is transmitted through the upper atmosphere to the troposphere is one of the important tasks in the problem of solar–terrestrial relations. Comparative study of the upper atmospheres of different planets and, in particular, of the dissipation of gases from the atmospheres assists in clarifying the problem of the evolution of planetary atmospheres.

Because the upper atmospheres are subject to such great variation (basically due to the solar activity), it is necessary to make numerous experiments under different conditions and construct models that describe the variation in the structure and the dynamics as a function of the determining factors. Among the information about the atmospheres of Venus and Mars obtained in recent years by means of space probes, the data on their upper atmospheres occupy an important position. At the same time, terrestrial observations and theoretical calculations of models have been made and these have assisted the interpretation of the experimental data and made it possible to predict the atmospheric conditions encountered by descending space probes.

In this review, we summarize and analyze critically the existing experimental data on the upper atmospheres of Mars and Venus and the theoretical models constructed to describe them. We point out the obscurities and contradictions that remain in the description and the problems that thus arise.

In Ch. 2, we give the mean altitude distributions of the basic structural parameters of the atmospheres of Mars, Venus, and the Earth and we point out the main factors that govern these distributions. In Ch. 3, we consider the experimental data on the upper atmospheres of Venus and Mars. In Ch. 4, we describe the theoretical formalism used to study the upper atmospheres and also the main atomic and molecular processes that occur in them. In Ch. 5, we consider theoretical models of the structure and dynamics of the upper atmospheres and confront them with the experimental data. For readers using the data on the upper atmospheres, Chs. 2 and 5 are of the main interest and to some extent Ch. 3 in order to understand the accuracy and reliability of the experimental data. For those who are interested in the methods of theoretical description of the upper atmospheres, the assumptions and simplifications made, and the problems which remain in this field, Chs. 4 and 5 will be helpful.

Data on the upper atmospheres are accumulating very rapidly; they can be found in a great many papers, of which only a certain minimum can be cited in the present review, and they are also contained in a number of reviews published in recent years.[1–9] Some of the data contained in these reviews are already outdated. Inevitably, the data in the present review will be out of date after a certain time, especially in view of the fact that the Soviet probes Venera 9 and Venera 10 are currently on their way to Venus and the American Viking 1

TABLE I.

	Venus	Earth	Mars	Jupiter
Mean distance from the Sun, a.u.	0.723	1	1.524	5.203
Period of revolution, terrestrial days	224.7	365.26	687.0	4332.6
Eccentricity of orbit	0.0068	0.0167	0.0934	0.0484
Mean radius, km	6050	6370	3385	~70 000
Mass, in terrestrial masses	0.814	1	0.107	317.4
Density, g/cm^3	5.25	5.52	3.97	1.33
Acceleration of gravity on the surface, cm/sec^2	878	978	372	2300–2700
Angle of inclination of equator to plane of orbit, deg	0–2°	23°27′	23°57′	3°4′
Solar days	118 Earth days	23.93 h	24.62 h	9.93 h
Solar flux, $erg \cdot cm^{-2} \cdot sec^{-1}$	$2.66 \cdot 10^6$	$1.39 \cdot 10^6$	$6 \cdot 10^5$	$5.14 \cdot 10^4$
(rel. Earth)	1.91	1	0.428	0.037
Integrated spherical albedo	0.77	0.29–0.35	0.26	0.45–0.50
Main atmospheric components	CO_2	N_2, O_2	CO_2, Ar	H_2
Mean pressure at surface, atm	100	1.0	$6.0 \cdot 10^{-3}$	—
Mean temperature at surface	750 °K	290 °K	210 °K	—
Equilibrium temperature T_{eq}	228	251	218	105

Data mainly taken from[10]; some corrections from later sources.

and Viking 2 are on their way to Mars. However, I hope that the greater part of the information given in this review is reliable and that the review will help both those who use the data on the upper atmospheres and those who take part in the further development of planetary aeronomy.

2. GENERAL PICTURE OF THE STRUCTURE OF THE ATMOSPHERES OF THE TERRESTRIAL PLANETS

It is well known that the terrestrial planets—Venus, Earth, and Mars—are similar as regards a number of the astronomical parameters that influence the atmospheric characteristics (distance from the Sun, size, mass) and differ greatly from Jupiter and the other giant planets (see Table I). However, there are a number of important differences between them: the fast rotation about an axis of the Earth and Mars and the slow retrograde rotation of Venus, which results in a duration of solar day on Venus equal to about 118 terrestrial days; the small eccentricity of the orbit of Venus and small inclination of its equator to the plane of the orbit, leading to the absence of seasonal variations in its atmosphere, and the large eccentricity of the orbit of Mars; the pronounced magnetosphere of the Earth and the much weaker magnetospheres of Venus and Mars. Although the flux of solar radiation on Venus is almost twice, and on Mars less than half, the flux on the Earth, the large albedo of Venus and the small albedo of Mars decrease the influence of this difference, so that there is little difference between the equilibrium temperatures (see Table I). On the other hand, the structural parameters of the lower atmospheres are very different: The atmosphere of Venus is much hotter and denser than the atmosphere of the Earth while the atmosphere of Mars is much colder and more rarefied. Finally, the atmospheres of Mars and Venus consist basically of carbon dioxide but the atmosphere of the Earth consists mainly of nitrogen and oxygen. These differences indicate that the atmospheres have evolved differently. Comparison of the temperature of the surface and the equilibrium temperature shows that there is an especially strong greenhouse effect on Venus and less strong one on the Earth.

Let us consider the distributions of the atmospheric temperature T with altitude h on Venus, Earth, and Mars (Fig. 1). These distributions reflect the specific properties of the different atmospheric layers and they are used to introduce the names given to these layers. We should point out immediately that in Fig. 1 we give the mean, most probable distributions constructed from data of different accuracy and reliability; these data will be considered below. As can be seen from Fig. 1, the lowest layer in the atmospheres of all three planets—the troposphere—is characterized by a decrease of the temperature with altitude. The thermal regime of the troposphere is governed by the convective transport of heat into the atmosphere from the surface of the planet, which is heated by the visible and infrared solar radia-

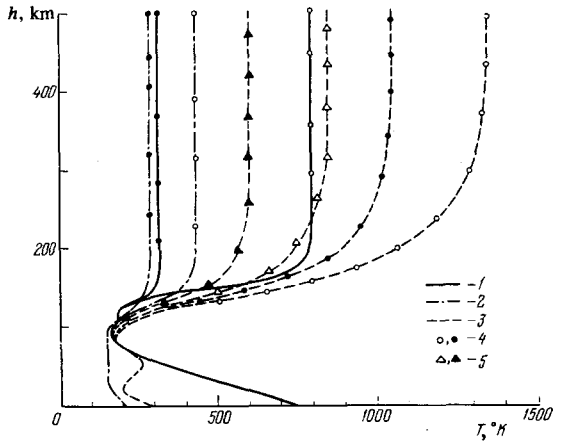

FIG. 1. Profiles of the temperature in the atmospheres of Venus (1), Mars (2), and the Earth (3) for high (4) and low (5) solar activity, during the day (open symbols) and by night (solid symbols).

tion, an appreciable fraction of which passes through the atmosphere. Above the troposphere, radiative transfer becomes important (because of the increase in the mean free path of infrared photons due to the lower density), the temperature gradient decreases, and the temperature profile gradually becomes isothermal. On the Earth, the temperature again increases with the altitude up to $h \approx 50$ km, where there is a maximum $T \approx 270-290$ °K (due to the absorption of the near ultraviolet by ozone). The region extending approximately from $h = 11-16$ to $h = 50-55$ km is called the stratosphere. Then, at altitudes from 50–55 to 80–90 km (this region is called the mesosphere) T again decreases to $T_{85} \approx 170-130$ °K. On Mars and Venus (where there is no maximum on account of the low ozone concentration) it is appropriate to refer to the entire region in which radiative transfer is predominant as the mesosphere (although on some occasions it is called the stratosphere and in[11] Dickinson introduces for Venus both a stratosphere and a mesosphere, which are separated by a small temperature maximum obtained in calculations; see Fig. 22 below). On Mars the mesosphere is situated approximately between 30 and 70 km and on Venus approximately between 50 and 125 km. The equilibrium temperature T_{eq} is equal to the temperature near the mesopause (upper boundary of the mesosphere), whence infrared photons escape into outer space (cf. Table I and Fig. 1).

Above the mesopause, the temperature again increases with the altitude and its profile $T(h)$ then becomes isothermal. This region is called the thermosphere. Its thermal regime is governed by the absorption of ultraviolet and x-ray solar radiation and removal of energy by heat conduction downward into the mesosphere. In the upper thermosphere, the infrared radiation is negligibly small since collisions between molecules are so rare that there is no effective excitation of the molecular vibrational levels from which infrared photons are emitted (this is the phenomenon of so-called vibrational relaxation). Finally, at altitudes at which the mean free path l is greater than the scale height H_n ($1/H_n = -d\ln n/dh$; n is the concentration of particles) we have the exosphere—the outer region of the atmosphere, where the atoms move with virtually no collisions and the atoms that in their last collision near the thermopause (or the base of the exosphere at the altitude where $l = H$) acquired a velocity greater than the critical velocity leave the atmosphere (the so-called process of thermal dissipation), and the remainder move along ballistic trajectories and then return to the thermopause. The base of the exosphere is situated on the average at an altitude of about 500 km on the Earth, around 210–250 km on Venus, and around 180–230 km on Mars.

It can also be seen from Fig. 1 that in the thermosphere the thermal regime is so variable that one can conveniently consider several profiles corresponding to high and low levels of solar activity and also day and night conditions, whereas in the lower lying layers the changes are comparatively small and it is sufficient to consider only one mean curve.

In Fig. 2, we compare for the Earth, Mars, and Venus the altitude profiles of the concentration, which decreases with altitude exponentially in accordance with the barometric formula

$$n(h) = n(h_0)\frac{T(h_0)}{T(h)}\exp\left(-\int_{h_0}^{h}\frac{Mg}{R_0 T}\,dh'\right), \qquad (1)$$

where R_0 is the universal gas constant, M is the molecular weight, g is the acceleration due to gravity, and h is the altitude. The density and pressure also decrease exponentially with the altitude in accordance with expressions analogous to (1).

It can be seen from Figs. 1 and 2 that the very large differences in the structure of the lower atmospheres (the much denser and hotter troposphere of Venus compared with the Earth and the much colder and more rarefied troposphere of Mars) decrease in the upper atmospheres, so that the concentrations in all three planets are similar at altitudes 129–150 km.

As we have already said, the atmospheres of Mars

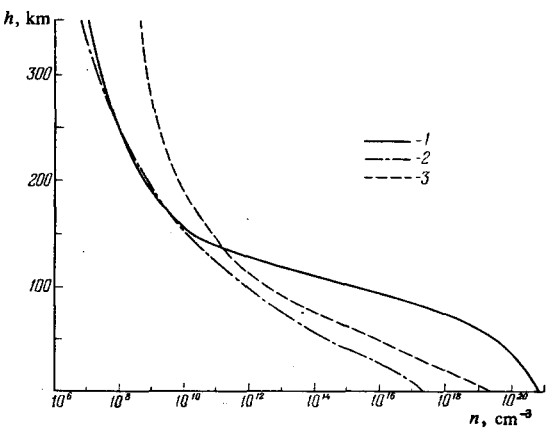

FIG. 2. Profiles of the concentration of neutral particles by day for high solar activity in the atmospheres of Venus (1), Mars (2), and the Earth (3).

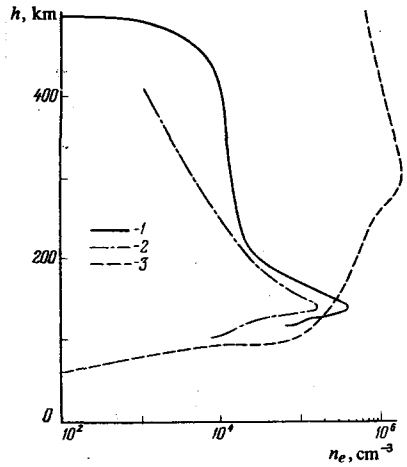

FIG. 3. Profiles of electron density in the ionosphere by day for high solar activity on Venus (1), Mars (2), and the Earth (3).

and Venus consist predominantly of CO_2, while the atmosphere of the Earth consists predominantly of N_2 and O_2. In the Earth's atmosphere, because of turbulent mixing, the composition does not change with altitude (the relative concentrations satisfy $n_k/n = \text{const}$, and the molecular weight $M = \sum_k M_k n_k/n = \text{const}$) from the surface to the altitude $h_T = 105 \pm 5$ km (homopause or turbopause; the region of constant composition in $h < h_T$ is the homosphere; the region of variable composition in $h > h_T$ is the heterosphere). In the homosphere, the concentration of each component is distributed with altitude in accordance with the barometric formula with scale height H_k determined by the mean molecular weight:

$$\frac{1}{H_k} = \frac{Mg}{R_0 T} + \frac{d \ln T}{dh},$$

whereas in the heterosphere there is a diffusion separation of the components, as a result of which each of them is distributed in accordance with the barometric formula with the scale height

$$\frac{1}{H_k} = \frac{M_k g}{R_0 T} + \frac{d \ln T}{dh},$$

i.e., the concentrations of the heavy components decrease with altitude faster than for the light components. There are indirect data (see below in Sec. C of Ch. 5) that in the atmospheres of Mars and Venus there are also homospheres and heterospheres, although the altitudes of the homopause are as yet known only very approximately. The change in the composition of the upper atmosphere is also governed by photodissociation: Beginning at a certain altitude, the atmosphere contains atomic oxygen O, and on Mars and Venus CO as well.

Short-wave solar photons with wavelengths shorter than 900–1000 Å ionize the atmospheric particles, giving rise to the ionosphere of the planet. The ionospheres of Mars and Venus are similar but very different from the Earth's (Fig. 3). The ionosphere of the Earth is more pronounced and extended, with concentrations (by day at a high solar activity) up to $(1-3) \cdot 10^6$ electrons and ions in a cubic centimeter at the principal maximum, which is situated on the average at an altitude of about 300 km. In contrast, the ionospheres of Mars and Venus occupy a much narrower range of altitudes, have a principal maximum on the dayside at an altitude of 140–150 km, where the concentration of electron–ion pairs is of order 10^5 cm^{-3}. On the nightside of Venus, the concentration at the principal maximum (which is situated at about the same altitude as on the dayside) is of order 10^4 cm^{-3}. In the nightside ionosphere of Mars, the concentration is about $5 \cdot 10^3$ cm^{-3}. These differences are explained, first, by the different composition of the neutral atmosphere and, second, by the presence of the strong magnetosphere of the Earth, which is about 10^4 times stronger than the weak magnetospheres of Mars and Venus (see Sec. F in Ch. 5).

3. EXPERIMENTAL DATA ON THE UPPER ATMOSPHERES OF VENUS AND MARS

A. Venus

Of great importance for the description of the upper atmosphere of Venus were the measurements of the parameters of its lower atmosphere (in particular the demonstration that CO_2 is predominant at $97 \pm 3\%$) by means of the gas analyzers on Venera 4–6 (see[12,13]) and also the measurements of the temperature and pressure made by Venera 4–8 ([2,14–17]) and the density and temperature measured by Mariner 5 and 10 ([18–23]), which made it possible to construct altitude profiles of the temperature and density to an altitude of about 90 km (see Figs. 1 and 2) and establish that to this altitude the temperature differs little on the day and night sides of the planet and varies little with the time.

The first measurements in the upper atmosphere of Venus were refraction measurements made when Venus occulted the star Regulus, from which it was determined, albeit with low accuracy, that at altitude 120 km the concentration is $n = 6 \cdot 10^{13}$ cm^{-3}, the scale height $H = 6 \pm 2$ km, and $T = 190–380$ °K ([24,25]).

A number of data on the upper atmosphere were obtained by Venera 4 and Venera 6, which entered the atmosphere of Venus on October 18, 1967 and May 16, 1969, and also by Mariner 5 and Mariner 10, which flew past Venus on October 19, 1967 and February 5, 1974, respectively.

Ultraviolet photometers and spectrometers on Venera 4 and 6 and Mariner 5 and 10 measured the altitude profiles of the emission intensity in various spectral lines and bands in the upper atmosphere of the planet, from which the concentrations of a number of the atmospheric components were determined with a certain accuracy.

The instruments measured the integrated (along the line of sight) intensity in the given line (or band) $I_\lambda^k(h)$. In principle, given $I_\lambda^k(h)$ one can, by solving an integral equation, find the volume luminosity $i_\lambda^k(h)$; if the layer of gas has a large optical thickness, it is also necessary to take into account multiple absorption and emission of photons. Then, from $i_\lambda^k(h)$ one can calculate the concentrations n_k of the emit-

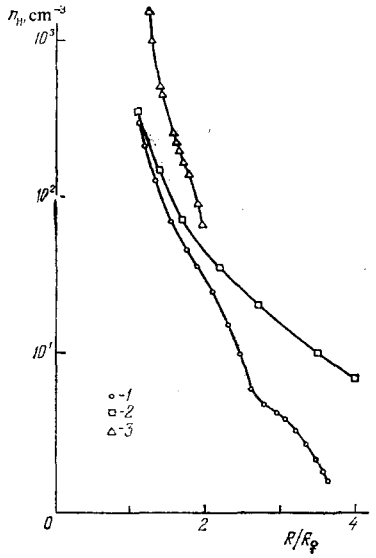

FIG. 4. Profiles of the concentration of hydrogen in the atmosphere of Venus according to the data of measurements by Venera 4 (1), Venera 6 (2), and Mariner 5 (3).

ting particles if one knows the mechanisms of their excitation, it being necessary to remember that one line may be excited by several mechanisms (resonant scattering of solar radiation, photodissociation and photoionization with excitation, impact excitation by photoelectrons, excitation resulting from dissociative recombination). As the finding of $n_k(h)$ from $I_\lambda^k(h)$ is not only complicated but also subject to large error, the procedure adopted in the majority of cases was as follows. First, on the basis of a model, altitude profiles of the concentrations $n_k(h)$ were specified and from them $i_\lambda^k(h)$ and $I_\lambda^k(h)$ calculated; then, comparing the calculated profiles $I_\lambda^k(h)$ with the experimental profiles and varying the parameters $n_k(h)$ of the model the best correspondence was achieved. It is true that in this case the solution is not unique since one and the same profile $I_\lambda^k(h)$ can be obtained by varying either the temperature profile $T(h)$ or the boundary value of the concentration $n_k(h_0)$; however, it is possible to obtain concentrations accurate to within a factor 2–3 and sometimes better (see, for example, Figs. 9 and 10 below).

Measurements of the scattered Lyman α radiation of hydrogen at 1216 Å by Venera 4 and 6 yielded the distribution of hydrogen in the nightside exosphere of Venus: from $n_H = 300$ cm^{-3} at the planetocentric distance $r = 6900$ km to $n_H = 1.5$ cm^{-3} at $r = 22100$ km (Fig. 4); the scale height of this profile corresponded to a temperature $T_{ex} \approx 300$ °K of the nightside exosphere.[26,27]

Analogous measurement on Mariner 5 on the dayside of the planet gave the profile $n_H(h)$, from the upper part of which $T_{ex} \approx 650$ °K at moderate solar activity, corresponding to $F_{10.7} = 120$[1)] ([28–30]), while Mariner 10 measurements gave $T_{ex} \approx 400$ °K at a low solar activity corresponding to $F_{10.7} = 75$ ([36]). Extrapolation of the experimental data gives $n_H(210) \approx 10^5$ cm^{-3} at the base of the exosphere.

The lower part of the $n_H(h)$ profile obtained from the Mariner 5 measurements at altitudes $h < 3000$ km had half the scale height H of the upper part; different explanations for this have been proposed, none of which is completely satisfactory (presence of a large amount of deuterium, two-temperature mixture of gases, and other explanations[31–34]), so that the fact itself has been doubted.[35]

From the emission intensity in the atomic oxygen line 1304 Å the concentration of atomic oxygen was estimated at from one to a few percent of the CO_2 concentration at the altitude 135–140 km; the problem is complicated by the large optical thickness ($\tau \sim 10^2$) and a certain uncertainty in the knowledge of the characteristic excitation mechanisms (this line is excited by resonant scattering of solar photons, photoelectron impact, and, to a certain extent, by dissociative recombination of CO_2^+).[37–40]

From the fact that no 1304 Å emission was detected on the nightside of Venus by Venera 4 it was concluded, with allowance for the sensitivity of the instrument, that at altitude $h \approx 300$ km and zenith angle $\chi \approx 107°$ of the Sun $n_0(300) \leqslant 2 \cdot 10^3$ cm^{-3} ([26,27]). However, Strickland has objected that the concentration could be greater and that the absence of emission could be explained by the photons not penetrating to this altitude at the given zenith angle because of the great optical thickness.[40]

On the dayside of Venus, 1304 Å emission was also measured from a rocket launched from the Earth to an altitude of 150 km, the intensity measured from approximately half the disk being equal to 11 kR during the flight on December 5, 1969 and 5.7 kR ($5.7 \cdot 10^9$ photons · cm^{-2} · sec^{-1}) during the flight on January 25, 1971.[41–44] On Mariner 10, the limb 1304 Å intensity was equal to 17 kR.[36] The oxygen concentration on the dayside of Venus estimated from these data ranges from a few to about ten percent of the CO_2 concentration at the altitude 135–140 km.

Mariner 10 also measured the emission intensity in the helium line 584 Å, which was equal to 0.61 kR. From this it was estimated that the helium concentration at altitude 200 km is of order 10^5 cm^{-3}.[36] In addition, Mariner 10 detected CO emission (4-th positive system of bands in the region of 1480 Å, 55 kR), C (1657 Å, 30 kR), and also Ar (867 and 1048 Å), Ne (740 Å), He^+ (304 Å), and strong unidentified emission in the region of 1500–1600 Å.[36]

Data on the profile of the electron density $n_e(h)$ in the ionosphere of Venus were obtained by the radar–occultation method when the space probe disappeared behind the planet and re-emerged.

When a radio wave passes through an atmosphere, the frequency, phase, and amplitude are changed. The neutral and charged components affect the refractive index differently; if radio waves of two frequencies are used,

[1)] As index of the solar activity one frequently takes $F_{10.7}$, the flux of solar radio radiation at the wavelength 10.7 cm, which is satisfactorily correlated with the ultraviolet solar flux that heats the upper atmosphere and with the sunspot number. This flux varies from $F_{10.7} = 65$–75 (in units of 10^{-22} W · m^{-2} · Hz^{-1}) at a low, to $F_{10.7} \approx 200$–250 at a high solar activity.

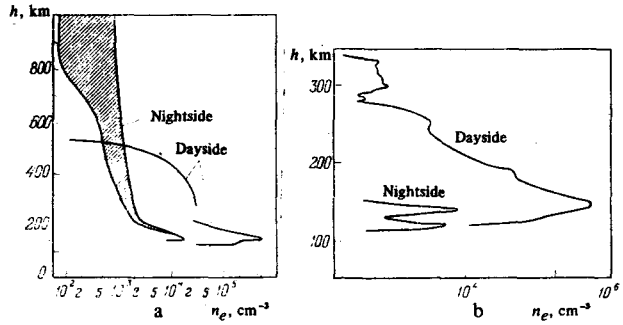

FIG. 5. Distribution of electron density in the ionosphere of Venus. a) High solar activity (according to data of Mariner 5), b) low solar activity (according to data of Mariner 10).

these influences can be readily distinguished. The majority of data on the ionosphere was obtained from the change in the phase shift resulting from passage of the radio waves through the ionosphere. The refractive index at given altitude, which depends on n_e, was obtained from an integral equation, a number of simplifying assumptions usually being made (spherical symmetry of the ionosphere, absence of multipath propagation, and others[21,22,46]). As a result of the simplifications, the error in the determination of $n_e(h)$ is rather large: In the best case it is of the order of tens of percent, but under unfavorable conditions it amounts to an order of magnitude.[47,48]

The electron density profiles obtained by the radar-occultation method with Mariner 5[21,22,49,50] (Fig. 5) show that in the dayside ionosphere there is maximum at altitude $h = 142$ km, where $n_{e\,max} = (5.5 \pm 0.5) \cdot 10^5$ cm^{-3}. Above the principal maximum, n_e decreases right out to 200 km with scale height $H = 28$ km. This scale height corresponds to a temperature of 630 °K ([51,52]), which agrees well with the temperature found from the scale height for the upper part of the hydrogen concentration profile. At approximately 200–400 km the scale height of the electrons is much greater, this obviously being due to the presence of light ions. At an altitude of about 500 km, there is a sharp drop in n_e—a "plasmopause"—(from $n_e \sim 10^4$ to $n_e \lesssim 10^2$ cm^{-3}), whose presence can be explained by compression of the ionosphere by the solar wind.[21,22,46] The nightside ionosphere had a maximum at approximately the same altitude as the dayside ionosphere, with $n_{e\,max} = 2 \cdot 10^4$ cm^{-3}, and then, to an altitude of about 200 km, n_e decreased with a constant scale height, after which, to about 10 000 km, n_e remained in the range 10^2–10^3 cm^{-3}.

The $n_e(h)$ profile measured at low solar activity during the flyby of Mariner 10 ([23]) (Fig. 5), had principal maximum $n_{e\,max} = 3 \cdot 10^5$ cm^{-3} at altitude $h = 145$ km and additional maxima at about 180 and 240 km; a plasmopause was noted near 350 km but less clearly expressed than in the Mariner 5 experiment. In the nightside profile, two peaks were discovered: one at 140 km with $n_e \approx 10^4$ cm^{-3} and another, separated from the first by a deep minimum, with a somewhat lower n_e at altitude 120 km.

Motions in the mesosphere of Venus, at altitudes 65–75 km, were first detected from the motion of the characteristic cloud details distinguished on photographs made on the Earth in the near ultraviolet, in the range 3500–3700 Å,[53–56] and then later a more detailed picture was obtained by means of television photographs through a filter with effective wavelengths $\lambda \approx 3550$ Å as Mariner 10 swung past Venus.[57] On the basis of these data, we obtain the following picture of the motions at the level of the cloud layer on Venus (Fig. 6): The atmosphere here rotates strongly, overtaking the rotation of the planet: The linear velocity of the surface of Venus with respect to the planet–Sun line is about 4 m/sec (which corresponds to solar days equal to about 118 terrestrial days) and the zonal (directed along parallels) component of the mesosphere velocity near the equator is $v_\varphi \approx 99$–100 m/sec (which corresponds to rotation around the planet in about four days). The zonal component of the velocity increases with increasing latitude, reaching about 200 m/sec at altitude 50°; at this latitude, the meridional component of the velocity is about 10 m/sec. The streamlines diverge from the equator to the pole. The cloud details indicate the presence of convective cells in the equatorial region and (even more developed) in the region around the subsolar point. These motions are evidently also present in the cloud layer itself: indeed, the altitude profile of the wind obtained by Venera 8 (Ref. 17) indicates an increase in the velocity from 50 to 80 m/sec at altitudes from 40 to 50 km.

A number of conjectures have been put forward[58–61] to explain the remarkable fact of the rapid rotation of the mesosphere of Venus. According to the most developed conjecture, this rotation develops as follows.[60] As a result of heating of the atmospheric gas by the solar radiation, convective cells arise, in which the gas rises at the subsolar point and sinks at the antisolar point. The major part of the heat is liberated near the lower boundary of the layer, and heat is transported upward by heat conduction; because of the finite thermal conductivity, the heating of the upper layers lags in phase behind the heating of the lower layers. This means that the isotherms and the convective cells are inclined to the side opposite to the motion of the source relative to the gas. As a result, there arises a vertical flux of the horizontal component of the momentum, which causes an increase with altitude of the mean horizontal velocity in the direction of rotation of the planet. Shubert and Young,[60] who have made numerical calculations in a simplified model, have shown that because of this effect the velocity in the mesosphere of Venus can indeed increase with altitude, reaching values near those ob-

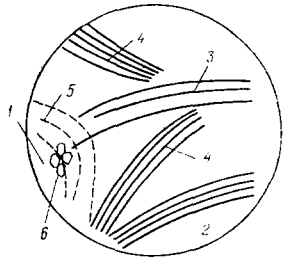

FIG. 6. Pattern of winds in the mesosphere of Venus deduced from television photographs in the ultraviolet taken by Mariner 10. 1) Subsolar region, 2) polar region, 3) equatorial bands, 4) spiral bands, 5) waves, 6) convective cells.

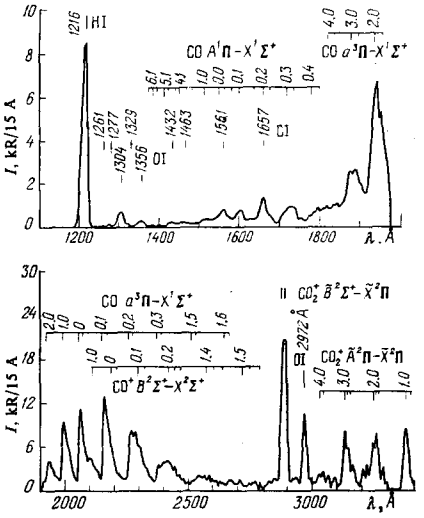

FIG. 7. Ultraviolet spectra of the emission of the atmosphere of Mars according to Mariner 9 measurements.

served. Analyzing the dimensionless numbers that govern the solution of the problem, they also concluded that such a rotation cannot occur on Mars or on the Earth.

B. Mars

The atmosphere of Mars (like Venus) consists predominantly of CO_2 (up to 65–95%, as was established by comparing different experimental data[6,8,10]). According to the data of the mass spectrometer on Mars 7, the atmosphere of Mars contains 25–35% of an inert gas, most probably argon.[62] Of small components, there are: CO (relative volume concentration $n_{CO}/n_{CO_2} \approx 2 \cdot 10^{-3}$), O_2 ($\sim 10^{-3}$), H_2O ($\sim 10^{-3}$); indirect data also indicates that there may be N_2 ($5 \cdot 10^{-3}$–$5 \cdot 10^{-2}$), H_2 ($\sim 5 \cdot 10^{-5}$).

The rarefied lower atmosphere of Mars (mean pressure at the surface $p_0 = 6.0$ mb[45,87]) is subject to large temperature variations (diurnal and seasonal, as a result of which the temperature of the surface varies in the range 150–290 °K). The vertical profiles $T(h)$ are also variable, and the vertical temperature gradient is sometimes nearly adiabatic, while during dust storms the profile $T(h)$ at altitudes 0–30 km sometimes becomes almost isothermal. The variable lower atmosphere, in which there are obviously strong winds and

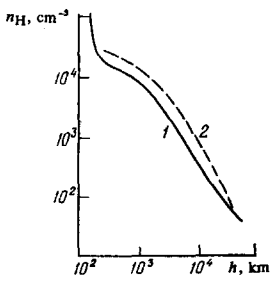

FIG. 8. Profiles of the concentration of atomic hydrogen in the atmosphere of Mars. 1) Data of Mars 3, 2) data of Mariner 6 and 7.

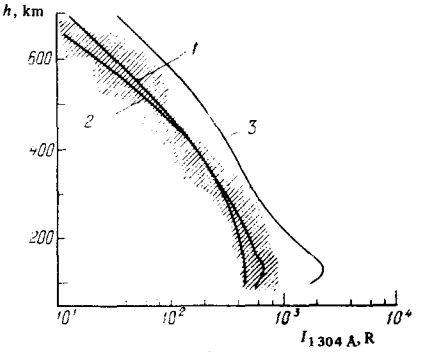

FIG. 9. Intensity of oxygen emission at λ1304 Å for $\chi_\odot = 44°$ as a function of the altitude from measurements by Mariner 6 and 7 (hatched region). The curves are taken from McElroy's models: 1) for $n_0(125) = 5 \cdot 10^7$, $T_\infty = 435$ °K; 2) for $n_0(125) = 1 \cdot 10^8$, $T_\infty = 364$ °K; 3) for $n_0(125) = 6 \cdot 10^8$, $T_\infty = 364$ °K.

turbulence,[63,64] must have a strong dynamical influence on the upper atmosphere (there are indirect proofs of this; see below).

A large number of experimental data on the upper atmosphere of Mars were obtained by the Mariner and Mars space probes. The data on the ultraviolet atmospheric emissions obtained by means of the photometers on the latter[65–69] and the Mariner spectrometers[70–74] have made it possible to calculate the vertical profiles of the concentrations of a number of the atmospheric components, determine the temperature from their scale heights, and also clarify the role played by various physical and photochemical processes taking place in the upper atmosphere. Figure 7 shows the spectra obtained by Mariner 9 and the identified emissions.

From the emission of the atmosphere in Lyman α (1216 Å) the vertical profiles of the hydrogen atoms for August 1969 were calculated from the data of Mariner 6 and 7 ([75]) and for January 1972 from the data of Mars 3 ([65,66,69]) (Fig. 8). The temperature of the exosphere corresponding to these distributions is $T_\infty = 300$–350 °K. The appreciable differences in n_H (by a factor 1.5 at altitude 250 km) were explained in[65,66] by the large variations of n_H in the atmosphere of Mars, since atomic hydrogen appears in the atmosphere mainly as a result of photodissociation of H_2O, and infrared spectrometers revealed variations of the H_2O concentration on Mars in the range from about 10 to 70 μm precipitated water.[76,77]

To estimate the concentration of atomic oxygen, the lines 1304, 1356, and 2972 Å were used.[37–39,78] In the majority of these investigations, an estimate was found for the relative concentration of oxygen at the altitude of the ionospheric maximum, i.e., at altitude 135–140 km; this concentration lies in the range $n_0(135) = (0.5$–$3\%)n_{CO_2}$, i.e., $n^0 = 5 \cdot 10^7$–$8 \cdot 10^8$ cm^{-3}. According to the results of Mars 6, $n_0(100) = (2$–$8) \cdot 10^9$ cm^{-3}.[67] To a considerable degree, these discrepancies reflect the influence of the errors of the measurements, the uncertainties in the characteristics of the processes (see above in connection with the measurements on Venus), and the ambiguity in the determination of the profile $n_0(h)$ resulting from the choice of the model (see, for example, Fig. 9, which shows that the intensity profiles

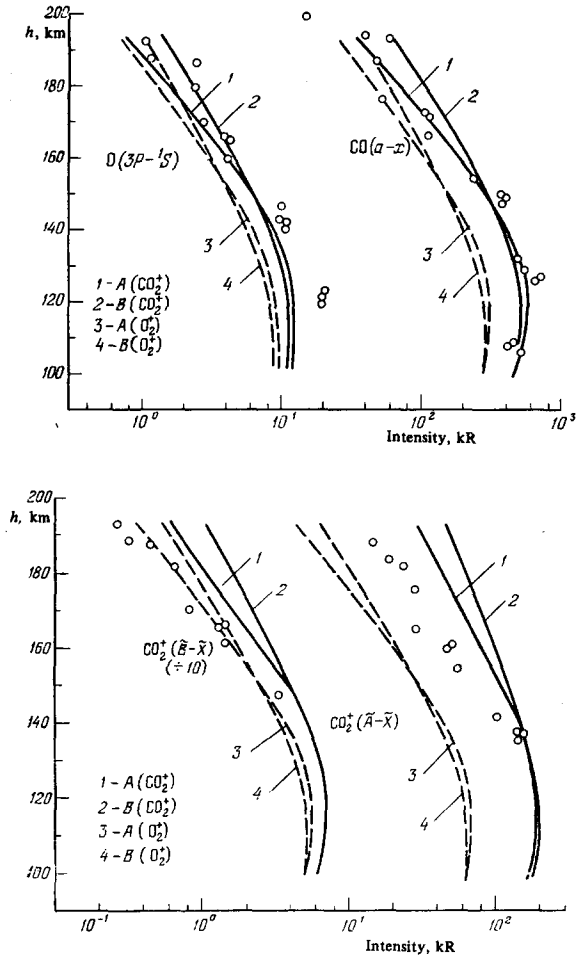

FIG. 10. Intensity of ultraviolet emissions on Mars from experiments and models. Models 1–4 under different assumptions about the recombination processes and the predominant ions.[82]

$I_{1304}(h)$ measured by Mariner 6 and 7 are equally well described by $n_0(125) = 5 \cdot 10^7$, $T_\infty = 435$ °K or $n_0(125) = 1 \cdot 10^8$, $T_\infty = 364$ °K). However, in estimating these discrepancies one should not forget that to a considerable degree they may reflect real variations in the oxygen concentration, particularly as a function of the solar zenith angle and the solar activity, as follows from theoretical models.

It is very difficult to determine the CO concentration. The detected emissions—the Cameron bands ($a^3\Pi - X^1\Sigma$) and the 4-th positive system of bands ($A^1\Pi - X^1\Sigma$) are generated basically in the dissociation and excitation of CO_2 by electrons and photons (as a result of which the profiles of these emissions have a scale height equal to that of CO_2 and not CO). Thomas,[38] analyzing the distribution of the intensity over the vibrational levels, estimated that the concentration of CO relative to CO_2 at altitude 135 km is approximately 0.3–1%.

From the emission of carbon in the lines 1561 and 1657 Å it has been estimated[79] that the concentration of carbon atoms at altitudes 150–200 km is of order $n_C \sim 10^4$ cm^{-3}.

From the absence of nitrogen emission in the spectra obtained by Mariner 6 and Mariner 7 and with allowance for the sensitivity of the instrument it has been shown that 0.5–5.0% nitrogen can be present in the atmosphere of Mars (depending on the mixing conditions; the value is probably closer to the lower limit).[80,81]

The emission of the ion $CO_2^+(A^2\Pi_u - X^2\Pi_g)$ and $(B^2\Sigma_u^+ - X^2\Pi_g)$ has been used to estimate the concentration of this ion at altitudes 130–200 km.[82,83] It has been concluded (with allowance for radar-occultation electron density data) that the CO_2^+ ion constitutes about 30% and the O_2^+ ion about 70% of the total number of ions.

As we have already noted, the altitude profiles of the emission in the Cameron band have the CO_2 scale height. From the measurements on Mariner 6 and 7 this was used to obtain the scale height $H_{CO_2} = 19 \pm 4.5$ km, corresponding to $T_\infty = 335 \pm 75$ °K. It is true that allowance for other emissions led to the conclusion that the best value is $T_\infty \approx 350$ °K.[82]

Similar measurements on Mariner 9 made it possible to follow the variations of H_{CO_2} and hence T_∞ for about a month, during which the index of solar activity varied in the range $F_{10.7} = 109$–145.[73] These data reveal the following facts, which are important for understanding the thermal regime of the thermosphere: The intensity of the CO emission ($a - X$) is well correlated (correlation coefficient 0.8) with $F_{10.7}$ (Fig. 11a), whereas H_{CO_2}, and therefore T, at altitude 150–200 km does not depend clearly on $F_{10.7}$, although it undergoes very strong variations (Fig. 11b), fluctuating from 14.8 to 24.3 km with mean value 17.8 km (which corresponds to variations of T (150–200) from 270 to 445 °K with mean value 325 °K). At the same time, according to the model of[82] the scale height for the given variation of $F_{10.7}$ must change by only 2 km. We shall discuss these facts a little later.

The radar-occultation experiments performed by Mariner 4, 6, 7, and 9 and Mars 2–6 made it possible to measure the electron density profile $n_e(h)$ in the ionosphere of Mars.[84–95] Some of these profiles obtained with Mars 2, 4, and 6 are shown in Fig. 12. Figure 13 shows the variations with altitude of the principal ionospheric maximum h_{max}, the electron density at the principal maximum $n_{e\,max}$, and the scale height of the electrons H_e above the maximum during the period of operation of Mariner 9 (first 80 revolutions; November–December 1971 and the following; May–June, 1972).

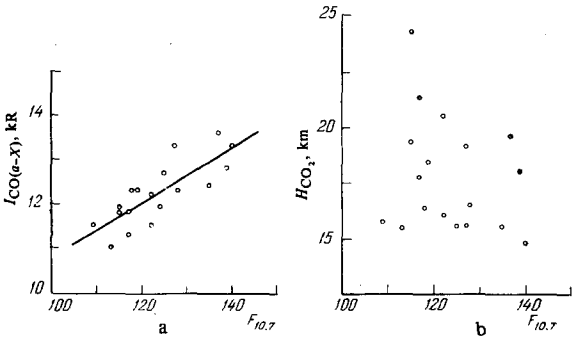

FIG. 11. Intensity of emission in the band CO ($a - X$) (a) and scale height of CO_2 (b) as a function of the solar activity index $F_{10.7}$.

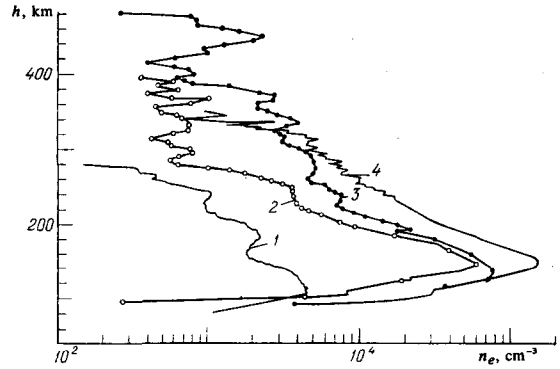

FIG. 12. Profiles of electron density in the ionosphere of Mars based on radar-occultation with Mars 2, 4, and 6. 1) At night ($\chi_\odot = 127°$, Feb. 10, 1974, 2) evening ($\chi_\odot = 82°$, Feb. 10, 1974), 3) evening ($\chi_\odot = 72°$, March 12, 1974), 4) by day ($\chi_\odot = 50°$, December 18, 1971).

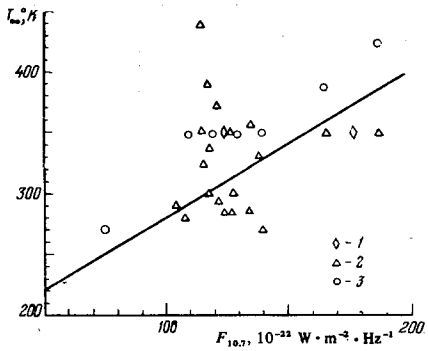

FIG. 14. Temperature of the upper thermosphere of Mars T_∞ as a function of the solar activity. 1) Deduced from the hydrogen scale height, 2) from the CO_2 scale height, 3) from the plasma scale height.

The radar-occultation data show that at the principal ionospheric maximum, which occurs at an altitude between 120 and 150 km (depending on the solar zenith angle and the level of solar activity) the dayside electron density (at $\chi \approx 50°$) is approximately equal to (1–2) $\cdot 10^5$ cm^{-3}, near the terminator it is (4–8) $\cdot 10^4$ cm^{-3}, and at night (at $\chi = 127°$) it is $n_e = 4.6 \cdot 10^3$ cm^{-3}. A number of profiles exhibit an additional maximum 20–30 km below the principal maximum. In Fig. 13 it can be seen that whereas $n_{e\,max}$ and h_{max} vary in agreement with the theoretical model (dashed curve, though the agreement does get worse at large χ), the variations of H_e are more complicated: In the first period of measurements, H_e did not change strongly about the almost unchanged average value $H_{av} \approx 38$ km (the CO_2 scale height behaved in approximately the same way; see Fig. 11) although the level of solar activity changed appreciably ($F_{10.7} = 109$–145). In the second period one can see that there was an appreciable increase in H_e (approximately from 25 to 50 km), whereas $F_{10.7} \approx 100$–170. These facts can be explained as follows. If one summarizes the data on the temperature (Fig. 14)[96] determined from the scale heights of hydrogen, the electrons, and CO_2 as determined by the experiments with Mariner 4, 6, 7, and 9 with solar activity varying from $F_{10.7} = 75$ to $F_{10.7} = 190$, the dependence of T_∞ on $F_{10.7}$ becomes obvious: At low solar activity $T_\infty \approx 250$–270 °K and at high activity $T_\infty \approx 350$–400 °K. This dependence can be described by the expression $T_\infty \approx 1.2F_{10.7} + 160$, though it should not be forgotten that, because of the small amount of data, the coefficients need to be made more accurate (nevertheless, this dependence is, in my opinion, more accurate than the one proposed by Steward and Hogan[97]). At the same time, it can be seen from Fig. 14 that at the end of 1971 (when $F_{10.7} \approx 100$–140) this dependence was blurred. This can be explained by the influence of an additional heat source. This could be, as is noted in[74], dissipation of gravity waves arriving from the troposphere, which could have been particularly intensive because of a global dust storm on Mars at that time.

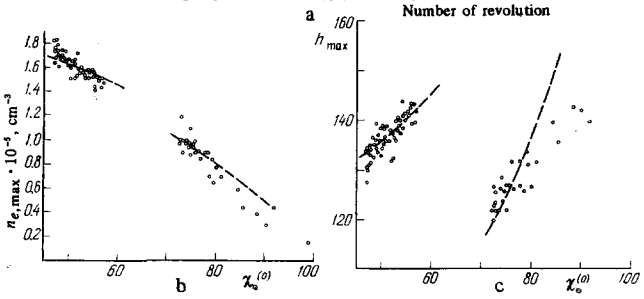

FIG. 13. a) Variation of scale height of electrons above the ionospheric maximum with the time; b) dependence of the electron density at the ionospheric maximum on the zenith angle of the Sun; c) dependence of the altitude of the ionospheric maximum on the zenith angle of the Sun. The circles are experimental points and the dashed lines are deduced from models.

4. FUNDAMENTALS OF THE THEORETICAL DESCRIPTION OF THE UPPER ATMOSPHERE

The diversity and complexity of the processes that occur in the upper atmosphere lead to the use of numerous simplifications in the construction of models. It is helpful to consider first the general formulation of the problem, which will make it easier later to evaluate the simplifications used to calculate concrete models.

A. System of equations for describing the structure and dynamics of the upper atmosphere

The upper atmosphere of a planet is a multicomponent mixture of rarefied gases subjected to the periodic influence of short-wave solar photons, which give rise to photodissociation, photoionization, and a number of other processes that ultimately heat the gas, change its composition, and generate motions in it.[98–104] At the same time, since the particle concentration n decreases exponentially with altitude, the mean free time increases as $\tau_0 \approx (n\sigma v_T)^{-1}$ (σ is the collision cross section and v_T is the mean thermal velocity), which is equal in order of magnitude to the time required to establish equilibrium with respect to the translational degrees of

freedom. The time required to establish equilibrium with respect to the vibrational degrees of freedom of the molecules is several orders of magnitude longer. Some chemical reactions have much longer characteristic times. As a result of the operation of several processes at great altitudes there is a departure from local thermodynamic equilibrium, which is expressed in a difference between the temperature of the ions, electrons, and neutral particles[104,105,159,207,210] and possibly in a certain difference between the temperatures of the neutral components on Mars and Venus,[106] and in a difference, under certain conditions, between the vibrational and kinetic (translational) temperature of nitrogen[107]; in the constant presence of chemically active components (such as O, O_3, and others) and particles with excited metastable energy levels[99,104,108]; finally, in deviations from Kirchhoff's law and of the emission of the atmosphere at thermospheric altitudes from the Planck distribution.[11,109,110]

A complete description of such a system is possible by means of a system of modified Boltzmann equations for each component of the atmosphere (with collision integrals for both elastic and inelastic processes) and the equation of radiative transfer.[100-103] However, such a description is not only too complicated but also too detailed: In a number of problems one needs to know, not the complete distribution function, but only its moments describing the macroscopic parameters of the atmosphere.

To considerable heights in the thermosphere (as long as the mean free path l of the molecules is much less than the scale height H and the mean free time is much shorter than the characteristic time of the problem under consideration) the thermal regime, the composition, and the motion of the upper atmosphere can be described by a system of hydrodynamic equations of Navier–Stokes type.[101-103] This system is obtained from the Boltzmann equations by successive multiplication of those equations by the masses, momenta, and energies of the particles and integration over the velocity space.[111,112] It is true that in the upper thermosphere (where the Knudsen number $K = l/H$ lies approximately in the range $0.2 \leq K < 1$) one should strictly speaking use the Boltzmann equation since under these conditions the heat flux vector and the viscous stress tensor are determined with a certain error in the Navier–Stokes approximations; however, this error is here not very important since the mass, momentum, and energy fluxes are so great that over short characteristic times diffusion equilibrium is established with isothermal temperature profiles and velocity field that is homogeneous in altitude (see Sec. A of Ch. 5). In addition, comparison of the theory with certain experiments in rarefied gases shows that the Navier–Stokes equations are suitable for fairly large values of K (almost up to $K \approx 1$).[239] A different way of describing the upper atmosphere is also used—by means of the equations of Grad's 13-moment approximation,[100,240] it being assumed that these equations hold to larger K values than the Navier–Stokes equations. However, from various papers one can conclude that the equations of the higher approximations, like the Navier–Stokes equations, are valid only for sufficiently small K, though they may give a more detailed description of certain effects.[241,242] The description of the exosphere (where $K > 1$) is simpler because here one can use the collisionless Boltzmann equation.[212]

In the system of Navier–Stokes equations, the continuity equations for each of the components of the atmosphere have the form

$$\frac{\partial n_k}{\partial t} + \operatorname{div}(n_k \mathbf{v}_k) = P_k - L_k, \tag{2}$$

where n_k and $\mathbf{v}_k$ are the concentration and velocity of the particles of the component k, t is the time, P_k and L_k are the rate of appearance and disappearance of the particles k in chemical and photochemical reactions (see Sec. B of Ch. 4); the particle flux $n_k\mathbf{v}_k$ is made up of the transport of particles with the mass velocity of the gas $\mathbf{v} = \rho^{-1}\sum \rho_k \mathbf{v}_k$ (ρ is the density), the diffusion velocity $\mathbf{V}_k$ and, below the homopause, also by turbulence $\mathbf{v}'_k$, i.e.

$$n_k \mathbf{v}_k = n_k \mathbf{v} + n_k \mathbf{V}_k + \overline{n'_k \mathbf{v}'_k}, \tag{3}$$

We write the diffusion flux in the approximation of a small component and we neglect diffusion along horizontals compared with mass transport:

$$n_k \mathbf{V}_k = -D_k n_k \left[\frac{\partial \ln n_k}{\partial r} + \frac{M_k g}{R_0 T} + (1+\alpha)\frac{\partial \ln T}{\partial r} \right], \tag{4}$$

where D_k is the diffusion coefficient (for the charged component, the coefficient of ambipolar diffusion[243,244]), α is the thermal diffusion factor[112]; M_k is the molecular weight of component k, and r is the vertical coordinate The turbulent flux of particles can be represented in the form[113,114]

$$\overline{n'_k \mathbf{v}'_k} = -D_T n_k \left(\frac{\partial \ln n_k}{\partial r} + \frac{\bar{M} g}{R_0 T} + \frac{\partial \ln T}{\partial r} \right), \tag{5}$$

where D_T is the coefficient of turbulent mixing, $\bar{M}$ is the mean molecular weight, $\bar{M} = n^{-1}\sum_k M_k n_k$. In the atmosphere of the Earth, D_T has been determined experimentally,[115-118] while for Mars and Venus there are only estimates of its magnitude (see the section in Ch. 5). Comparison of (4) and (5) shows that whereas molecular diffusion tends to distribute each component in accordance with its scale height H_k (as occurs in the heterosphere, where $D_k > D_T$), turbulent mixing tends to distribute all the components with the single scale height $\bar{H}$ determined by the mean molecular weight $\bar{M}$ (as occurs in the homosphere, where $D_T > D_k$). The homopause is situated at the altitude where $D_k = D_T$; on the Earth, $h_k = 105 \pm 10$ km; on Mars and Venus the altitudes of the homopause are as yet known only approximately (see Sec. C in Ch. 5).

An equation of motion can be written down conveniently for all of the neutral gas by summing the equations of motion for the components, which gives

$$\rho\left(\frac{\partial \mathbf{v}}{\partial t} + (\mathbf{v}\nabla)\mathbf{v}\right) + \operatorname{grad} p - \operatorname{div}\Pi = \rho \mathbf{g} + \frac{1}{2}\rho \nu_{ni}(\mathbf{v}_i - \mathbf{v}), \tag{6}$$

where p is the pressure, Π is the viscous stress tensor, ρ is the density, $\mathbf{v}$ and $\mathbf{v}_i$ are the velocities of the neu-

tral particles and the ions, ν_{ni} is the frequency of neutral–ion collisions,[245,246] $\mathbf{g}$ is the vector of the acceleration of gravity,

$$\Pi_{\alpha\beta}=\eta\left(\frac{\partial v_\alpha}{\partial x_\beta}+\frac{\partial v_\beta}{\partial x_\alpha}-\frac{2}{3}\frac{\partial v_\gamma}{\partial x_\gamma}\delta_{\alpha\beta}\right),$$

and η is the coefficient of viscosity.

The equations of motion for the ions and the electrons are analogous to (6) with the addition on the right-hand side of the Lorentz force $\pm en_{i,e}(\mathbf{E}+(1/c)[\mathbf{v}_{i,e}\times\mathbf{B}]$, where e is the electron charge, $\mathbf{E}$ is the electric field, c is the velocity of light, and $\mathbf{B}$ is the magnetic field of the planet), and the replacement of ν_{ni} by the corresponding collision frequencies.[243,244,247] The last term in (6) is important on a planet that has an appreciable magnetic field, which, influencing the ions, can give rise to a difference between the drift velocity $\mathbf{v}_i$ and the wind velocity $\mathbf{v}$.

If one uses a coordinate system rotating with the planet (which is more convenient for local problems, whereas for global problems a nonrotating system is more convenient), then to the right-hand side of (6) one must add the Coriolis force $-2\rho[\omega\times\mathbf{v}]$ (ω is the angular velocity of rotation of the planet); the centrifugal force on the planets of the terrestrial group is small and usually included in $\mathbf{g}$ (which then becomes a function of the latitude).

The energy balance equation for the neutral gas obtained by summing the equations for the components can be written in the form

$$\rho\left[\frac{\partial(c_vT)}{\partial t}+(\mathbf{v}\nabla)(c_vT)\right]-\nabla(\varkappa\nabla T)+p\,\mathrm{div}\,\mathbf{v}-\Pi:\left(\frac{\partial\mathbf{v}}{\partial\mathbf{r}}\right)=Q_S$$
$$-Q_{IR}+Q_{\mathrm{ch}}+\frac{1}{4}\rho\nu_{ni}(v_i-v)^2+\frac{3}{4}kn\nu_{ni}(T_i-T)+3kn\nu_{ne}\frac{m_e}{m}(T_e-T); \quad (7)$$

where $c_v=\rho^{-1}\sum c_{vk}\rho_k$; k is Boltzmann's constant; $\varkappa$ is the thermal conductivity coefficient; Q_S is the source of heat due to the absorption of solar ultraviolet radiation; Q_{IR} is the heat sink due to the infrared emission of the atmosphere; Q_{ch} is the heat source due to chemical reactions; T_e and T_i are the electron and ion temperatures; ν_{ne} is the frequency of neutral–electron collisions; m_e is the electron mass; m is the mean mass of the neutral particles (approximately equal to the mean mass of the ions).

Analogous equations can be written down for the electron and ion gases.[244,248–250] The heat source for the electron gas is the energy transmitted to it by the thermalization of the photoelectrons. The electron gas gives up an appreciable fraction of its heat to the ions; the ion gas, an appreciable fraction to the neutral gas. Therefore, in a wide range of altitudes in the thermosphere $T_e>T_i>T$.[104,105,159,207,210,248–250]

The possibility of considering just one energy balance equation for the neutral gas is due to the fact, as a rule, the temperatures of the neutral components T_k differ negligibly little. However, some exceptions are possible: According to the estimates of[106], on Mars and Venus the temperature of the light components, hydrogen and helium, differ appreciably (by 50–100°) from the CO_2 temperature; to calculate these effects, energy balance equations for the individual components are used.

In the homosphere, Eq. (7) is augmented by the gradient of the heat flux q_T due to turbulent heat conduction[118–120]:

$$q_T=-\rho c_pD_T\left(\frac{\partial T}{\partial r}+\frac{g}{c_p}\right) \quad (8)$$

and the heat source due to dissipation of the turbulent energy[120]:

$$\varepsilon_T=\frac{D_T g\rho}{\mathbf{Ri}_c T}\left(\frac{\partial T}{\partial r}+\frac{g}{c_p}\right). \quad (9)$$

where $\mathbf{Ri}$ is the Richardson number. According to the estimate of[120] (under the assumption of a critical value $\mathbf{Ri}_c\approx0.2$) the influence of ε_T is predominant, but according to[252] we have $\mathbf{Ri}_c\approx1$ and q_T has a greater influence on the thermal regime than ε_T.

The heat source due to the absorption of solar ultraviolet radiation Q_s, for concentrations n_k of the absorbing components distributed in accordance with the barometric formula (1), can be represented in the form[104,121]

$$Q_s(r,\chi)=\sum_k\int\varepsilon(\lambda,r)F_{\lambda\infty}\sigma_kn_k\exp\left[-\sum_k\sigma_kn_kH_k\,\mathrm{Ch}(\chi,X)\right]d\lambda, \quad (10)$$

where $F_{\lambda\infty}$ is the spectral flux of the solar radiation at the boundary of the atmosphere, σ_k is the cross section for the absorption of photons by particles of component k, λ is the wavelength of the photons, $\mathrm{CH}(\chi,X)$ is the Chapman function, which takes into account the curvature of the atmospheric layers[104,122]; χ is the zenith angle of the Sun, $X=r/H$ (r is the planetocentric radius), and ε is the heating efficiency, i.e., the fraction of the photon energy that goes over into heat (see Sec. C of Ch. 4).

The infrared heat sink in the atmospheres of the Earth, Mars, and Venus is due almost entirely to the emission of photons in the 15-μ CO_2 band and for an optically thin layer can be represented in the form[123]

$$Q_I=h\nu nn_{CO_2}\eta_v\exp\left(-\frac{h\nu}{kT}\right)F(x), \quad (11)$$

where $h\nu$ is the photon energy, η_v is the parameter of vibrational relaxation (a function of the temperature), $F(x)$ is the screening function

$$F(x)=1-(1+x)e^{-x}.\quad x=(10^9/n_{CO_2})[1+(A/n\eta_v)],$$

A^{-1} is the radiation lifetime of the band. A maximum of Q_{IR} lies near the mesopause and its values decrease rapidly at both higher and lower altitudes. The expression (11) satisfactorily approximates the infrared sink in the thermosphere, though to calculate the thermal regime of the mesophere it is necessary to take into account multiple emission and absorption of infrared photons by solving the equation of radiative transfer[11,110] (see Sec. B of Ch. 5). The infrared sink, which carries into space heat that arrives both from

above and below, facilitates the separate treatment of the thermal regime of the thermosphere and mesosphere. The source Q_{ch} can become appreciable only in the upper mesosphere.[251]

Although the absorption of ultraviolet solar radiation is the main heat source in the thermosphere, additional sources are possible. First, by the dissipation of atmospheric gravity waves arriving from the lower atmosphere; this source is appreciable on the Earth and there are also indirect indications that it may be important on Mars, especially during global dust storms. Second, due to the energy transmitted to the atmosphere from the plasma flux of the solar wind; this source is important on the Earth, especially at high latitudes and during geomagnetic disturbances; its value on Mars and Venus has not yet been investigated.

In the description of the global variations of the structure of the upper atmosphere (i.e., variations with horizontal scales equal to the radius r_0 of the planet, vertical scales equal to or greater than the scale height H, and time scales of the order of a day or more) the system of equations admits a further important simplification.[102,103] For this, the equations are reduced to dimensionless form with allowance for the various scales and one calculates the values of the dimensionless numbers (the Mach number **M**, the Reynolds number **Re**, and the Strouhal number **S**) from model values of the structure parameters and allowance is made for the quasihorizontal motions, i.e., the fact that the ratio of the vertical, v_r, and horizontal, v_h, velocities satisfies $v_r/v_h \sim H/r_0 \ll 1$ (which is confirmed by model calculations and, for the Earth, by experiments as well). One then makes a comparative estimate of the terms of the equations and ignores the terms that have order 10^{-2} and smaller compared with the main terms. As a result, in the continuity equations only the vertical components of the diffusion fluxes are important and in the energy equation only the vertical component of the heat flux due to heat conduction; in addition, in the energy equation there is a considerable simplification of the term $\Pi : \partial \mathbf{v}/\partial \mathbf{r}$, which describes the work of the viscous forces and which can be expressed in the form $\eta[(\partial v_\varphi/\partial r)^2 + (\partial v_\vartheta/\partial r)^2]$ (v_φ and v_ϑ are the zonal and meridional components of the velocity, r is the planetocentric radius, φ is the longitude, and θ is the colatitude). In the horizontal projections of the equation of motion the form of the viscous stress tensor appreciably simplifies, and the equations become equivalent to boundary layer equations; for example, the equation for the zonal component v_φ takes the form

$$\rho\left(\frac{\partial v_\varphi}{\partial t} + v_r\frac{\partial v_\varphi}{\partial r} + \frac{v_\theta}{r}\frac{\partial v_\varphi}{\partial \theta} + \frac{v_\varphi}{r\sin\theta}\frac{\partial v_\varphi}{\partial \varphi} - \frac{v_\varphi v_\theta}{r}\operatorname{ctg}\theta\right) = -\frac{1}{r\sin\theta}\frac{\partial p}{\partial \varphi} + \frac{\partial}{\partial r}\left(\eta\frac{\partial v_\varphi}{\partial r}\right) + \frac{1}{2}\rho\nu_{ni}(v_{i\varphi} - v_\varphi). \quad (12)$$

The equation for v_ϑ has a similar form.

The vertical projection of the equation of motion (for motions with scales $L \geq H$ and such that $\mathbf{M}^2 \ll 1$) goes over into the equation of quasistatics:

$$\frac{\partial p}{\partial r} = -\rho g. \quad (13)$$

From Eq. (13) and the equation of state in Clapeyron's form

$$p = nkT \quad (14)$$

the barometric formula (1) follows.

We emphasize that it does not follow from (13) that the vertical velocity v_r can be ignored, as it is in a number of models. The vertical velocity plays an important role, giving rise to an additional source and sink of heat accompanying adiabatic compression and expansion of gas in the gravitational field. In calculations, v_r is determined basically by the continuity equation.[195,196]

The boundary conditions for the system of equations that describe the structure and dynamics of the upper atmosphere are specified on the upper boundary on the basis of the absence of fluxes of energy, momentum, and mass to infinity (in the continuity equations for the light gases, allowance is made for their dissipation from the atmosphere); at the lower boundary one usually specifies empirical values of the structure parameters.

B. Elementary processes determining the energy sources and composition of the upper atmosphere

Short-wave (ultraviolet and x ray) solar photons, absorbed in the atmosphere, cause photodissociation and photoionization of the atmospheric atoms and molecules, including excitation of the quantum energy levels of the resulting particles. The excitation energy is either reemitted or (from metastable levels) transmitted to other particles by impact deactivation. The dissociation products may once more associate in triple collisions (or, with much smaller probability, as a result of radiative association), but this process has an appreciable probability at rather low altitudes (in the mesosphere), and therefore the dissociation products first diffuse from the thermosphere into the mesosphere. Many dissociation products are chemically very active and in the upper atmosphere a whole series of chemical reactions therefore takes place. Since the energy of the photons absorbed in the thermosphere reaches several hundred electronvolts, of which 10–12 eV are expended on the photoionization event, and since practically the entire excess energy is carried away by the photoelectron (because $m_i \gg m_e$), the photoelectron can, in a collision with particles, ionize them as well (giving rise to secondary, tertiary, and so forth, electrons) and also cause dissociation and excitation; in these processes, the electrons lose energy and are thermalized. The resulting ions react with the neutral particles and disappear as a result of recombination with the electrons.

In these processes, some of the energy of the absorbed photon goes over into heat, which is the main source of heating of the upper atmosphere. These processes also determine the neutral and ionic composition of the upper atomosphere.

Let us consider the actual processes that take place in the atmospheres of Mars and Venus, which consist predominantly of CO_2.

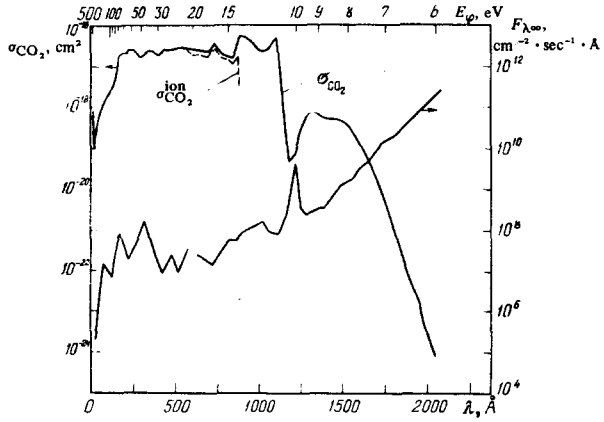

FIG. 15. Dependence of the spectral solar flux $F_{\lambda\infty}$ (photons $\cdot$ cm$^{-2}\cdot$ sec$^{-1}\cdot$ Å) averaged over an interval of 50 Å, the absorption cross section σ_{CO_2} of CO_2, and the cross section of photoionization $\sigma^{ion}_{CO_2}$ on the wavelength λ and the photon energy E_φ.

The flux of solar ultraviolet radiation with wavelength $\lambda \gtrsim 2500$ Å, which is absorbed in the upper atmosphere and gives rise to the above processes, consists of a continuum and lines (which arise in the photosphere, the chromosphere, and the corona of the Sun) and varies considerably with the solar activity, the amplitude of the variations increasing strongly with decreasing λ.[124,125] The magnitude of this flux in different spectral regions has frequently been measured with rockets and satellites and these data have made it possible to plot the dependence $F_{\lambda\infty}(\lambda)$ (Fig. 15) for different levels of the solar activity.[126–130] However, the danger has been pointed out[129] that, because of experimental difficulties, the dependence $F_{\lambda\infty}(\lambda)$ is known with an appreciable error. Improvement in the accuracy of this quantity is very important for the majority of problems in aeronomy.

The cross section for the absorption of radiation by CO_2 molecules, which has been measured in the laboratory,[131–134] is very large ($\sigma_{CO_2} \sim 10^{-17}$ cm^2) in the range $\lambda \approx 150$–1000 Å and is still large ($\sim 10^{-19}$ cm^2) until about $\lambda \approx 1600$ Å (see Fig. 15, in which we have also plotted the ionization cross section $\sigma^{ion}_{CO_2}(\lambda)$ according to laboratory measurements[135]).

The absorption of photons in the wavelength range 2274–902 Å occurs in the photodissociation process

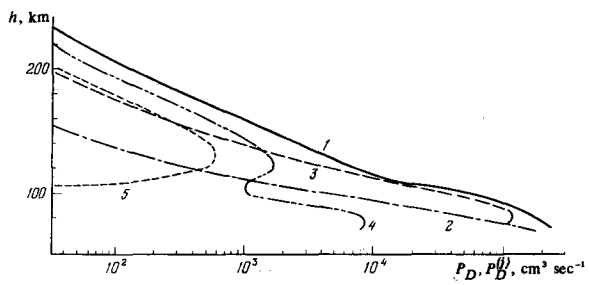

FIG. 16. Total rate of photodissociation of CO_2 in the atmosphere of Mars, P_D, and rate of photodissociation with excitation through different channels, $P_D^{(j)}$, for zenith angle $\chi_\odot = 0$ of the Sun. 1) P_D, 2) $P_D^{(1)}$, 3) $P_D^{(2)}$, 4) $P_D^{(3)}$, 5) $\sum_j P_D^{(j)}$ ($j > 4$).

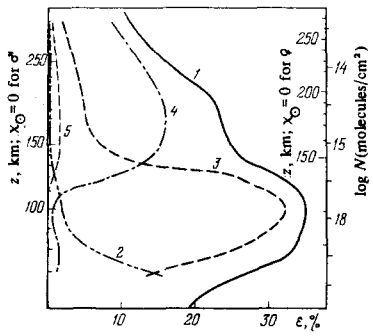

FIG. 17. Heating efficiency associated with photodissociation in the atmosphere of Mars and Venus: ε_D is the total, $\varepsilon_D^{(j)}$ is the contribution through individual channels. 1) ε_D, 2) $\varepsilon_D^{(1)}$, 3) $\varepsilon_D^{(2)}$, 4) $\varepsilon_D^{(3)}$, 5 $\sum_j \varepsilon_D^{(j)}$ ($j \geq 4$).

$$CO_2 + h\nu \rightarrow CO_2^* + O^*. \qquad (15)$$

Photons with $2274 \geq \lambda > 1670$ Å gives rise to the formation of molecules and atoms in the ground states of CO ($X^1\Sigma^+$) and O (^3P) (channel 1 in Figs. 16 and 17); photons with $1670 \geq \lambda > 1286$ Å form CO (X) and O (^1S) (channel 2); photons with $\lambda \leq 1286$ Å form CO (X) and O (^1S) (channel 3), the quantum efficiency of the reaction being near unity.[136–141] Photons with shorter wavelengths can excite also certain levels of CO ($a^3\Pi$, $a'\Sigma^+$, $d^3\Delta$, $e\Sigma^-$), although the probabilities of excitation of these channels ($j \geq 4$) are small,[142,143] obviously as a result of nonconservation of spin, so that the contribution to the photodissociation rate is slight (Fig. 16) and the contribution to the energy release is negligibly small (Fig. 17),[114] though these probabilities do need to be made more precise for a better description of the atmospheric emissions.

An important role in the energy balance of the upper atmosphere is played by particles in metastable states formed as a result of photodissociation with excitation (and also as a result of the other processes considered below). For example, the energy of the metastable levels O (^1D) and O (^1S) can be either emitted in the following transitions:

$$O(^1D) \rightarrow O(^3P) + h\nu \quad (\lambda = 6300 \text{ Å}), \qquad (16)$$
$$O(^1S) \rightarrow O(^1D) + h\nu \quad (\lambda = 5577 \text{ Å}), \qquad (17)$$
$$O(^1S) \rightarrow O(^3P) + h\nu \quad (\lambda = 2972 \text{ Å}) \qquad (18)$$

(with very long radiative lifetimes $\tau_R = A^{-1}$, where A is the Einstein radiation coefficient: $\tau_R(16) = 120$ sec; $\tau_R(17) = 0.74$ sec; $\tau_R(18) = 12$ sec) or go over into the kinetic energy of the particles and ultimately into heat (and partly also into vibrational energy of the molecules) as a result of impact deactivation or quenching:

$$O(^1D, {}^1S) + M \rightarrow O(^3P) + M, \qquad (19)$$

where M is any particle (on Mars or Venus, mainly CO_2); the coefficients have the values $k^{O(^1D)}_{CO_2} = 2.1 \cdot 10^{-10}$ cm^3/sec, $k^{O(^1S)}_{CO_2} = 2.5 \cdot 10^{-14}$ cm^3/sec.[145–147] The relative efficiency of these two channels depends on the height z. For example, the fraction of excited particles that undergo deactivation is

$$\Phi_j(z)=\frac{\sum k_\alpha^j n_\alpha}{A_j+\sum k_\alpha^j n_\alpha}. \quad (20)$$

The state CO ($a^3\Pi$) is also metastable, though its radiative lifetime is so short ($\tau_R=7.5\cdot10^{-3}$ sec) that its energy is almost completely re-emitted at all heights, giving the system of Cameron bands. The energy of the states CO ($a'^1\Sigma^+$, $d^3\Delta$, $e^3\Sigma^-$) is re-emitted through allowed transitions to the state CO ($a^3\Pi$).

The rate of photodissociation of CO_2 through individual channels and the total rate can be represented in the form

$$P_D(z)=\sum P_D^{(j)}(z)$$
$$=n_{CO_2}(z)\sum_j\int_0^{\lambda_{max}^j}\sigma_D^{(j)}(\lambda)\frac{F_{\lambda\infty}}{h\nu}\exp\Big[-\sum_\alpha\sigma_\alpha n_\alpha H_\alpha \mathrm{Ch}(\chi,X)\Big]d\lambda. \quad (21)$$

The dependences $P_D^{(j)}(z)$ and $P_D(z)$ calculated in this manner for Mars[144] are shown in Fig. 16, from which it can be seen that at altitudes greater than about 130 km the contribution of channel 3 is predominant, at altitudes of about 130–70 km it is channel 2, and at altitudes less than 70 km it is channel 1, and moreover, it can be seen from[37], in which a dependence similar to the one described here is obtained, that $P_D(h)$ increases monotonically with decreasing altitude right down to the surface of the planet. At the high rate of photodissociation of CO_2 on Mars and Venus, the opposite processes take place slowly. For example, the radiative association

$$CO+O\to CO_2+h\nu \quad (22)$$

has a rate $k_{22}\sim10^{-20}$ cm^3 sec^{-1}.[148,149] Association in the triple collisions

$$CO+O+M\to CO_2+M \quad (23)$$

has the rate $k_{23}=10^{-35}-10^{-37}$ cm^6 sec^{-1}.[150] At the same time, it is important that the reaction

$$O+O+M\to O_2+M \quad (24)$$

is much faster than the reaction (23): $k_{24}=10^{-33}$ cm^6 sec^{-1}.[151] Under these conditions, one encounters the problem of explaining why CO_2 is predominant in the atmospheres of Mars and Venus; this is discussed below

Photons with wavelengths shorter than 902 Å give rise to the photoionization

$$CO_2+h\nu\to CO_2^++e, \quad (25)$$

and photons with wavelengths shorter than 716 Å, 687 Å, and 640 Å cause ionization with excitation of the ion to the levels $A^3\Pi_u$, $B^2\Sigma_u^+$, and $C^2\Sigma_g^+$, respectively. Data on the partial cross sections for the individual channels of the reaction (25) as a function of the photon wavelength have been obtained by different methods in[152–155]. According to[154], the relative cross sections of ionization with excitation of the levels X, A, B, C at wavelength $\lambda=584$ Å are, respectively, equal to 22.6, 29.1, 44.8, and 4.3% and at λ 304 Å to 9.5, 10.5, 10.4, and 6.0%, respectively. The ratio of the cross sections of ionization with excitation of the levels of A and B is 0.69 according to measurements of the energy spectrum of the photoelectrons,[154] but 2.7 according to measurements of the fluorescence intensity.[155] This difference is explained by the fact that some of the molecules go over from state B to A because of the coupling of these two adjacent levels.[154]

The levels A and B decay, giving the bands $(A-X)$ and $(B-X)$, whereas virtually all molecules decay from level C into O^+ and CO as a result of predissociation.[156]

Photons with wavelengths shorter than 548 and 600 Å give rise to the dissociative ionization

$$CO_2+h\nu\to CO+O^++e, \quad (26)$$
$$CO_2+h\nu\to CO^++O+e. \quad (27)$$

In these reactions, according to the experiments of[157,158], the photons with $\lambda=584$ Å produce about 4% of the O^+ ions and about 2% of the CO^+ ions in the total number of ions; photons with $\lambda=304$ Å produce 18% O^+ and 12% CO^+ and photons with $\lambda=44$ Å produce 17% O^+ and 10% CO^+.

The photoelectrons from photoionization carry away virtually all the energy $E=h\nu-I_{CO_2}-W_{CO_2^+}^{(j)}$ (I_{CO_2} is the ionization potential and $W_{CO_2^+}^{(j)}$ is the excitation energy of level j of the ion) and give it up in elastic collisions (basically with the electron gas) and in inelastic collisions (in processes of excitation, dissociation, and ionization of particles by electron impact). Knowing the cross sections of these processes,[159,160] one can calculate the energy spectrum of the electrons $n_e(E)$,[80] the electron temperature T_e,[159,161] the fraction of the energy of the photons that goes over into heat as a result of photoionization (i.e., the heating efficiency) ε^{ion} ([159]) (see below, Sec. C of Ch. 4). The energy spectrum of the electrons on Mars at altitude 187 km calculated under a number of assumptions[80] exhibits a sharp decrease (by more than an order of magnitude) near $E=7$ eV, i.e., near the threshold of the excitation of the electron levels of CO_2.

The ion composition in the ionospheres of Mars and Venus is appreciably changed by the very fast ion–molecule reactions:

$$CO_2^++O\to O_2^++CO, \quad (28)$$
$$CO_2^++O\to O^++CO_2, \quad (29)$$
$$CO_2^++O_2\to O_2^++CO_2, \quad (30)$$
$$O^++CO_2\to O_2^++CO. \quad (31)$$

According to[162–164], the reaction rates are $k_{28}=1.6\cdot10^{-10}$, $k_{29}=1.0\cdot10^{-10}$, $k_{30}=5\cdot10^{-11}$, $k_{31}=1.2\cdot10^{-9}$ cm^3 sec^{-1}.

In addition, in the nightside ionosphere reaction with the participation of light ions are important; for example,

$$H^++CO_2\to COH^++O, \quad (32)$$
$$He^++CO_2\to O^++CO+He,$$
$$\to O+CO^++He \quad (33)$$

which have the rates $k_{32}=3\cdot10^{-9}$, $k_{33}=1.2\cdot10^{-9}$ cm^3 sec^{-1}.[165,166]

Ions and electrons disappear from the ionospheres of Venus and Mars basically in dissociative recombination reactions:

$$CO_2^+ + e \to CO^* + O^*, \quad (34)$$
$$O_2^+ + e \to O + O^* \quad (35)$$

and analogous reactions of light ions. The rates of these reactions are very high, $\alpha \sim 10^{-7}$ cm^3 sec^{-1}. For example, at room temperature $\alpha_{34}=3.8\cdot10^{-7}$ cm^3 sec^{-1}, $\alpha_{35}=2.0\cdot10^{-7}$ cm^3 sec^{-1}.[167,168] With increasing electron temperature they decrease: $\alpha \sim T^{-k}(k=1/2-3/2)$, and with increasing vibrational excitation of the ions they increase[169]; this last circumstance is important because vibrationally excited molecular ions can be formed in ion–molecular reactions in the ionosphere.

In dissociative recombination, the energy, which is equal to the difference between the ionization potential and the dissociation energy, $I_k - D_k$, goes over partly into excitation energy and partly into the kinetic energy of the resulting particles, and then into heat. This energy is appreciable (since $I_{CO_2}=13.6$ eV, $I_{O_2}=12.1$ eV, $D_{CO_2}=54.5$ eV, $D_{O_2}=5.10$ eV) and in different channels very different fractions of the energy go over into heat. The relative probabilities of these channels for the reaction (35) were measured in[170], according to which they are as follows: 0.5 for O(^3P), 0.45 for O(^1D), and 0.05 for O(^1S). In[171] it was found that in the reaction (34) approximately 5% of the CO molecules are formed in the state $A^1\Pi$ and the remainder in the state $X^1\Sigma$.

To explain the observed predominance of CO_2 in the atmospheres of Mars and Venus (bearing in mind its rapid photodissociation and slow recombination) a number of reactions have been proposed in which components containing hydrogen and chlorine catalyze the combination of CO and O.[6,7,172–179] The main reaction is

$$CO + OH \to CO_2 + H, \quad (36)$$

which has the fairly high rate $k_{36}=9\cdot10^{-13}\exp(-500/T)$.[180] The hydroxyl which participates in this reaction is formed in the cycle of reactions

$$H + O_2 + CO_2 \to HO_2 + CO_2, \quad (37)$$
$$O + HO_2 \to OH + O_2, \quad (38)$$
$$H + HO_2 \to 2OH, \quad (39)$$
$$HO_2 + HO_2 \to H_2O_2 + O_2, \quad (40)$$
$$HO_2 + h\nu \to OH + O, \quad (41)$$
$$H + O_3 \to OH + O_2, \quad (42)$$
$$H_2O_2 + h\nu \to 2OH. \quad (43)$$

The original atomic hydrogen for the reactions (37), (39), and (42) appears on Mars basically from the dissociation of water:

$$H_2O + h\nu - OH + H, \quad (44)$$

and on Venus from the photodissociation of hydrochloric acid, which has been discovered in spectroscopic experiments in the clouds of Venus,[181]

$$HCl + h\nu \to H + Cl, \quad (45)$$

the chlorine also having a catalytic action[172,173]:

$$Cl + O_2 + CO_2 \to ClO_2 + CO, \quad (46)$$
$$ClO_2 + CO \to ClO + CO_2, \quad (47)$$
$$ClO + CO \to Cl + CO_2. \quad (48)$$

Here we have listed only the main reactions; in calculations of models of the composition for Mars and Venus[172–179] (see also Sec. C of Ch. 5) between 20 to 50 reactions have been used.

To make more precise the picture of the neutral and ionic composition of the atmospheres of Mars and Venus further laboratory investigations of the rates of the reactions considered in this section are needed.

C. Heating efficiency

Consideration of the elementary processes in the upper atmosphere shows that only a certain fraction of the energy of an absorbed photon goes over into heat. This fraction of the energy (called the heating efficiency) is a function of the wavelength λ of the photon and the altitude h, and this function is different in the case of absorption of a photon due to photodissociation or photoionization.[121]

The heating efficiency in the case of photodissociation, $\varepsilon_D(\lambda, h)$, is more readily calculated.[144] Remembering that the number of photodissociation events in 1 cm^3 in a second is given by Eq. (21) and that in each event in which dissociation with excitation (in each channel j) occurs a fraction of the photon energy equal to $\varepsilon_D^{(j)}$ goes over into heat, the heat source due to photodissociation can be written in the form

$$Q_S(z) = \sum_j Q_S^{(j)} = n_{CO_2}(z) \sum_j \int_0^{\lambda_D} \varepsilon_D^{(j)}(\lambda, z)\,\sigma_D^{(j)} F(\lambda, z)\,d\lambda. \quad (49)$$

Although the integration is performed formally from 0 to the dissociation threshold λ_D, examination of the actual dependence $\sigma(\lambda)$ shows that it is sufficient to integrate over a spectral interval from about 600 to 2000 Å.

To obtain expressions for $\varepsilon_D^{(j)}(\lambda, h)$, it is necessary to bear in mind that the photon energy is transformed into heat in two ways ($\varepsilon_D^{(j)} = \varepsilon_{D_I}^{(j)} + \varepsilon_{D_{II}}^{(j)}$). First, the excess of the photon energy over the energy of dissociation and excitation goes over into kinetic energy of the resulting particles and then, through their collisions, into heat, i.e.

$$\varepsilon_{D_I}^{(j)}(\lambda) = \frac{h\nu - E_D - W_j}{h\nu}\varphi_j(\lambda), \quad (50)$$

where W_j is the energy of the level excited in channel j, φ_j is the factor decreasing the heating efficiency due to the excitation during CO_2 dissociation of vibrational–rotational CO levels whose energy is then emitted in the form of infrared photons (according to the estimates of[144], φ_j increases from $\varphi_j \approx 1/2$ for $\lambda > 1007$ Å to $\varphi_j \approx 1$ for $\lambda > 1286$ Å). Second, some of the excitation energy of the metastable levels goes over into heat as a re-

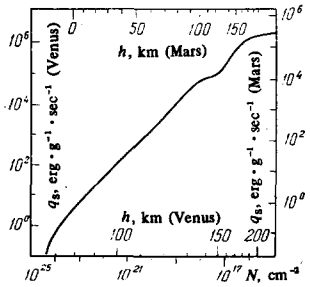

FIG. 18. Heat source due to absorption of solar ultraviolet radiation in the atmospheres of Mars and Venus, $q_s = Q_s/\rho$ (at moderately high solar activity ($F_{10.7} = 144$) and with heating efficiency $\varepsilon = 1$) as a function of the total number N of molecules on the path of the radiation. The altitudes h are given for $\chi_\odot = 0$.

sult of impact deactivation, i.e., if, for example, the level O(^1D) is excited in channel j, then

$$\varepsilon_{D\,\mathrm{II}}^{(j)} = \frac{W_{\mathrm{O}(^1D)} \sum_k k_{\mathrm{O}(^1D)}^k n_k}{h\nu\,(A_{\mathrm{O}(^1D)} + \sum_k k_{\mathrm{O}(^1D)}^k n_k)} \psi, \qquad (51)$$

where $k_{\mathrm{O}(^1D)}^k$ is the coefficient of impact deactivation of the level O(^1D) by particles of species k, and ψ is a factor that takes into account transition of some of the energy into vibrational degrees of freedom of CO_2 with subsequent de-excitation (according to estimates, the values of ψ lie in the range between 0.6 and 1.0). For channels in which the level O(^1S) is excited, the expression is analogous to (51), though somewhat more cumbersome. Generally speaking, it must be borne in mind that the energy expended on CO_2 dissociation goes over into heat as a result of association of CO and O, although estimates show that in the thermosphere this source can be ignored since association is effective in the mesosphere, whence the CO and O diffuse.

Figure 17 shows the function $\varepsilon_D = \sum_j \varepsilon_D^{(j)}$ calculated for an atmosphere of CO_2 as a function of the total number of particles in a column of unit section on the path of the photons, $N = nH\mathrm{CH}(\chi, X)$, and also as a function of the altitude on Mars and Venus (for $\psi = 1$, $\chi_\odot = 0$; for other values of χ one must calculate N and find $\varepsilon_0(N)$). It can be seen that ε_D varies from $\varepsilon_D \approx 0.3$ at altitude 100–120 km to $\varepsilon_D \approx 0.2$ at 200 km. One can also see that the contribution of the different channels varies with the altitude. According to approximate estimates, without allowance for the z dependence, the value $\varepsilon_D \approx 0.3$ was obtained in[182].

It is very difficult to calculate the heating efficiency in the case of photoionization, $\varepsilon_{\mathrm{ion}}$,[121] since some of the photon energy goes over into the thermal energy of the particles of the gas in many processes. First, this occurs in the impact deactivation of metastable levels of ions populated as a result of photoionization with excitation. Second, the photoelectrons, which carry away virtually all the photon's energy that exceeds the energy of photoionization and excitation, then lose this energy on ionization, dissociation, and excitation of particles (and metastable levels are also excited), and some of the energy is given up in elastic collisions to electrons of the ionosphere, from which some of the energy is transmitted to the neutral gas. Third, some of the energy expended on ionization goes over into thermal energy as a result of dissociative recombination of the ions.

A detailed calculation of $\varepsilon_{\mathrm{ion}}$ has not yet been made and there are only approximate estimates used to construct models of the thermosphere.[82,159,183–186] Henry and McElroy[159] obtained $\varepsilon_{\mathrm{ion}} \approx 0.6$, although examination of their assumptions shows that this is an overestimate. Shimizy[182] obtained $\varepsilon_{\mathrm{ion}} = 0.45$ with predominantly O_2^+ ions and $\varepsilon_{\mathrm{ion}} = 0.1$ with predominantly CO_2^+ ions. Stewart,[82] making the most probable assumptions, calculated a mean value $\varepsilon \approx 0.2$–0.3. Stewart and Hogan[188] selected a mean value of ε empirically (in such a way as to match the model scale height of the topside electrons to the experimental value) and obtained $\varepsilon \approx 0.3$. If the theoretical models of the structure of the thermosphere is to be made more accurate, we need more accurate calculations of $\varepsilon_{\mathrm{ion}}$, for which laboratory measurements of the characteristics of a number of the above elementary processes are required.

Figure 18 shows the heat source due to absorption of solar ultraviolet radiation in the atmospheres of Mars and Venus[189] per unit mass, $q_s = Q_s/\rho$, for a moderate to high solar activity (corresponding to $F_{10.7} = 144$) with $\varepsilon = 1$ (i.e., the values shown in Fig. 18 must be multiplied by the chosen value of ε); the altitudes for Mars and Venus are given for $\chi_\odot = 0$.

5. THEORETICAL MODELS OF THE STRUCTURE AND DYNAMICS OF THE UPPER ATOMSPHERES OF MARS AND VENUS

As was shown above (in Ch. 3), to calculate the structure and dynamics of the thermosphere it is necessary to solve a system of hydrodynamic equations with heat and particle sources, and in the mesosphere the system must be augmented by the equation of radiative transfer. Because of the complexity of the complete problem, a number of simplified models have been constructed, the following basic assumptions being made. First, calculations were made of the thermal regime or the composition without allowance for their coupling, the missing parameters being specified in accordance with empirical data. Second, the total spatially three-dimensional and nonstationary problem was replaced by a one-dimensional (stationary or nonstationary) or two-dimensional problem. Third, the hydrodynamic equations were linearized by ignoring the advective terms.

A. Models of the thermal regime and dynamics of the thermosphere

To solve the energy balance equation it is necessary to know the composition of the atmosphere, and therefore models constructed before the composition has been determined more accurately by the direct experiments[190,192] differ appreciably from the later models.

After it had been established experimentally that CO_2 is predominant in the atmospheres of Mars and Venus to great altitudes, a number of models were calcu-

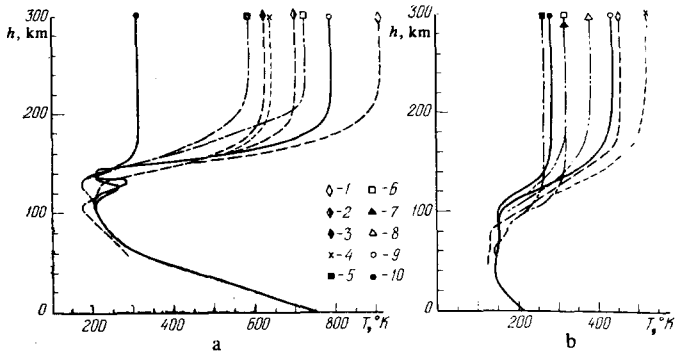

FIG. 19. Altitude distributions of the temperature in the atmospheres of Venus (a) and Mars (b). Models of[187] for high (1), average (2), and low (3) solar activity; models of[79] for moderately high solar activity (4); models of[193] for $\varepsilon = 0.25$(5) and $\varepsilon = 0.45$(b); models of[82] with predominance of CO_2^+(7) and O_2^+(8); models of [195,196] for moderately high solar activity: maximum by day (9), maximum by night (10).

lated[182–187,193] in which the vertical temperature profile $T(h)$ in a thermosphere of pure CO_2 (Fig. 19) was found by integrating the stationary one-dimensional energy balance equation, and the concentration profile was obtained from the barometric formula. At the lower boundary the temperature of the mesopause was specified in accordance with certain data, and at the upper an absence of heat flux was specified. The heat source Q_s was calculated from the approximate values of ε (as described in Sec. C of Ch. 4); the variation of Q_s with the solar activity was taken into account in a simplified manner by multiplying $F_{\lambda\infty}$ by some scale factor. To obtain the average profile the value $Q_s^* = (1/2)Q_s(\chi = 60°)$ was used. Comparison of the profiles obtained in this way with the profiles obtained in two-dimensional models shows that when Q_s^* is used one obtains a temperature that is close to the temperature near the terminator or to the average between the diurnal maximum and minimum of the temperature; this justifies the use of one-dimensional models to investigate certain effects. The differences between the $T(h)$ profiles obtained in the one-dimensional models are mainly due to the differences in allowing for Q_s.

The vertical temperature profile $T(h)$ calculated in[83] contains an appreciable temperature gradient in the upper thermosphere. This result needs to be confirmed since the calculation is complicated and may contain a large error (from the emission intensity $I_\lambda^*(h)$ integrated along the line of sight the volume luminosity $i_\lambda^*(h)$ is calculated; from it, the concentration profile $n_k(h)$, and from it $T(h)$). If this gradient is real, it could indicate that there is an appreciable heat flux from the solar wind through the magnetosphere into the atmosphere, transmitted, for example, by magnetohydrodynamic waves or by particle streams that penetrate into the magnetosphere.

In the model of[106] it was found from the solution of the system of energy balance equations for the individual components that the hydrogen and helium temperatures may deviate downward from the CO_2 temperature by approximately 50 °K on Mars and by more than 100 °K on Venus and that this difference depends strongly on the assumption made about the concentrations of the light gases and the amount of turbulent mixing in the lower thermosphere.

Attempts to describe the diurnal variations in the thermospheres of Mars and Venus in the framework of spatially one-dimensional nonstationary models were made in[106,182]; comparison of these results with the two-dimensional models show that the neglect in these models of the horizontal heat transport by winds leads to an overestimation of the diurnal variations.

To take into account the coupling between the thermal regime and the winds in the thermosphere, spatially two-dimensional models were constructed by numerical integration of the equations of motion, the energy equation, and the continuity equation. In the model of Dickinson for Venus[194] equations linearized by ignoring the advective terms (of the form $\mathbf{v}\nabla\mathbf{v}$) were used. In the models of Izakov and Morozov for Venus[195] and Mars[196] nonlinear equations were used. The models of[195,196] were constructed for a moderately high solar activity corresponding to $F_{10.7} \approx 150$ and heating efficiency $\varepsilon = 0.3$. The two-dimensional approximation (neglect of meridional spreading) restricts the applicability of the model of the equatorial thermosphere to the equinoctial period. Some other simplifications were made (atmosphere of pure CO_2, constancy of the coefficients $\varkappa$ and η), which, according to estimates, do not appreciably distort the resulting picture. First, one-dimensional distributions of the parameters were calculated and these were then used as initial conditions for integrating the spatially two-dimensional system with respect to the time until a stationary regime was established (in a nonrotating coordinate system with fixed planet–Sun axis), which was achieved after several terrestrial days. In Figs. 19 and 20, the continuous curves show a variant of the model of the thermosphere of Venus rotating with a period of four terrestrial days and the dashed curves show a nonrotating thermosphere (the v_θ and v_φ scales are displaced by 100 m/sec, which is approximately equal to the rotation velocity).

The temperature distribution in the upper thermosphere (at altitude 200 km) is characterized by a large difference between the temperature at the subsolar point (about 800 °K) and at the antisolar point (about 300 °K). At the same time, if the horizontal velocities were assumed equal to zero, the difference was even greater (about 920° and 150°), which indicates that the winds have an important influence on the thermal regime. As was pointed out above, the experimental data indicate $T_\infty \approx 400$ °K for $F_{10.7} = 75$ and $T_\infty = 650$ °K for $F_{10.7} = 120$, so that the model value $T_\infty \approx 800$ for $F_{10.7} = 150$ agrees well with these data.

Note that the temperature of the atmosphere of Venus at altitudes around 130 km according to the data of[195] (Fig. 19) is evidently overestimated because of inaccurate calculation of the infrared heat sink; here, the temperature profile of[11] is more accurate (Fig. 22b).

The winds in the upper thermosphere are character-

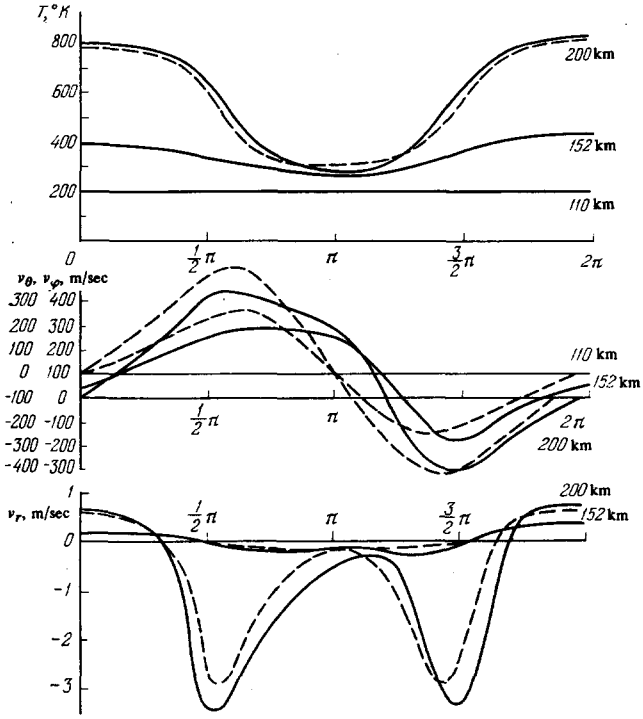

FIG. 20. Model of thermosphere of Venus rotating with a period of 4 terrestrial days (continuous curves) and nonrotating (dashed curves). Temperature T, horizontal velocities v_φ and v_θ, and vertical velocity v_r as functions of the angles φ and θ measured from the subsolar to the antisolar point (for the rotating therosphere the angle φ is measured in the equatorial plane in the direction of rotation). The scale of the velocity v_φ is shifted relative to the scale of v_θ by 100 m/sec (approximately by the rotation velocity).

ized by a flow of gas from about the subsolar point to the antisolar point with horizontal velocities up to 300–400 m/sec, these being maximal near the terminator. In the absence of rotation, there is a reverse flow at altitudes 120–130 km with velocities of about 10 m/sec, so that the total circulation of the thermosphere is a closed vortex. If rotation is superimposed, the vortex is displaced in the direction of the rotation (especially at the antisolar point) and is somewhat distorted. Gas rises on the dayside with vertical velocities of about 0.5 m/sec and sinks near the terminator and on the nightside with velocities up to 3.5 m/sec, these being maximal near the terminator. In Dickinson's model,[194] which has a certain similarity with the model described here, there are important differences in the distribution of the winds, this apparently being due to the linearization of the equations.

The analogous model for Mars[196] shows that in the absence of winds (dashed curves in Fig. 21) heating would take place from the rising to the setting of the Sun whereas in the presence of winds (continuous curves) the amplitude of the diurnal variation of the temperature is reduced, so that T_∞ is changed from about 280 to 430 °K (Figs. 19 and 21) for $F_{10.7}=150$, and the maximum and the minimum occur at earlier times. The horizontal projection of the wind at night is in the direction of rotation of the planet and its magnitude reaches 100 m/sec, while in the day it is in the direction opposite to the rotation and reaches 150 m/sec; the vertical projection of the wind is upward in the day and downward at night, and reaches 1 m/sec.

Thus, the theoretical models of the thermospheres enable one, despite the simplifications used in their calculation, to obtain temperature distributions that in the upper part agree satisfactorily with the experimental values of T_∞ and in the lower with the models of the mesosphere. It has been shown that winds appreciably affect the thermal regime, decreasing the amplitude of the diurnal variations, this especially strongly in the more slowly rotating thermosphere of Venus. It is true that the agreement between T_∞ and the experimental values was achieved by a semiempirical specification of Q_3, for which the errors in $F_{\lambda\infty}$ and in ε may mask each other.

To improve the description of the thermal regime and the dynamics of the thermospheres the following are needed: measurements of the spectral flux of the solar ultraviolet radiation at different levels of solar activity; exact calculations of the heating efficiency; experimental and theoretical study of the additional sources in the thermosphere; calculations of spatially three-dimensional nonstationary models of the thermosphere.

B. Models of the thermal regime of the mesosphere

The mesosphere is the region of the atmosphere for which it is hardest to make a model. Strictly speaking, to describe it one must solve simultaneously the equations of hydrodynamics and the equation of radiative transfer, the latter being complicated by the fact that here there is a marked deviation from local thermodynamic equilibrium, so that the emission function differs from the Planck distribution. At the same time, the experimental study of the mesosphere structure is also

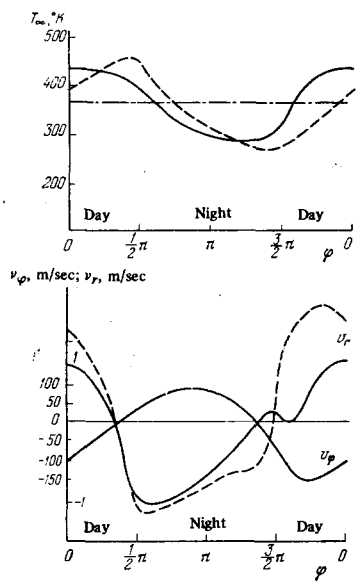

FIG. 21. Model of thermosphere of Mars. The continuous curves are with allowance for the horizontal velocities v_φ; the dashed, without allowance for v_φ.

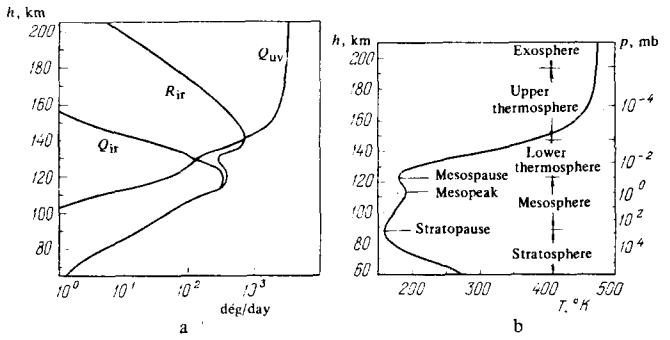

FIG. 22. Altitude profiles of heat sources and sinks in the mesosphere of Venus (a) and temperature profile calculated from them (b) by Dickinson. Q_{uv} and Q_{ir} are the heat sources due to the absorption of ultraviolet and infrared solar photons, R_{ir} is the heat sink due to infrared emission in the 15-μ CO_2 band.

difficult.

In a number of studies in which the temperature profiles of Mars and Venus have been calculated, mainly in the thermosphere but also partly in the mesosphere,[82,182–187,193] the cooling by infrared emission was calculated usually in the approximation of an optically thin layer with allowance for vibrational relaxation (in accordance with Eq. (11)), although sometimes the equation of radiative transfer was integrated under many simplifications; in some investigations, approximate allowance was also made for the absorption of infrared solar radiation.

In Dickinson's model of the mesosphere of Venus[11,197] a detailed analysis was made of the transfer of infrared radiation with allowance for the structure of the absorbing vibrational–rotational CO_2 bands, the changes in the line profiles as a function of the pressure, and also with allowance for the deviation from local thermodynamic equilibrium. Dickinson first found the mean global profile $T(h)$ (in a one-dimensional model)[11] with a simultaneous calculation of the heating due to the absorption of infrared solar radiation and cooling due to infrared emission, and he then calculated the deviations from the mean global heating and cooling.[197] The profiles of the global mean rates of heating by infrared solar radiation (basically due to absorption in the 2.0 and 2.7 μm bands) and cooling by infrared photons (mainly by emission in the 15-μ band) together with the heat source due to the absorption of solar ultraviolet radiation are shown in Fig. 22a.[11] It can be seen that the rates of heating by ultraviolet radiation and cooling by infrared emission are approximately equal at altitudes 130–140 km, where their magnitude reaches several hundred degrees per terrestrial day. It can also be seen that an appreciable part of the heating by infrared solar photons (with maximum at 115–125 km) is compensated by the infrared emission of the atmosphere.

The mean global profile of the temperature on Venus calculated in[11] with allowance for these heat sources and sinks is shown in Fig. 22b. The mesopause, with temperature around 180 °K, is at altitude 122 km; at an altitude of around 87 km there is a temperature minimum 158 °K, which Dickinson calls the stratopause; at 113 km there is additional maximum (around 180 °K, called the mesopeak by Dickinson).

The approximate calculation of the horizontal variations of the infrared heating and cooling[197] (with allowance for only the variation of the solar zenith angle with a constant vertical temperature profile corresponding to the global average conditions) showed that the horizontal variations of the infrared heating and cooling reach a factor two; the diurnal variations of the temperature at altitudes 111–112 km are equal to about 20°.

It follows from Dickinson's calculations that the frequently adopted estimate according to which the deviations from local thermodynamic equilibrium occur at altitudes where $A > n\eta_v$ is very inaccurate. On Venus, $A = n\eta_v$ at 86 km, and an appreciable deviation from local thermodynamic equilibrium begins only at about 125 km, where n is three orders of magnitude less than at 86 km. This occurs because, despite the greater ease with which the excitation energy of vibrational levels is emitted rather than thermalized at altitudes greater than 86 km ($A > n\eta_v$), the mean free path of the infrared photons is still very short, so that they are repeatedly absorbed and re-emitted, sustaining a near-equilibrium level population.

C. Models of the composition of the atmosphere

The empirical models of the composition[72,79,81] constructed from the experimental data on the concentrations of the components at a certain altitude or on the total concentration of a component using model profiles of the temperature and the barometric formula (an example of such a model for Mars is shown in Fig. 23, which comes from[81]) showed that both on Mars and on Venus the CO_2 concentration in the thermosphere exceeds the O concentration to great altitudes. This is a remarkable fact, since estimates showed a high rate of photodissociation of CO_2 and a low rate recombination of CO and O. In the theoretical models of[37,198], which were constructed by numerical integration of the system of continuity equations (2) under a number of simplifying assumptions, CO and O concentrations close to the experimental were obtained under the assumption of very strong turbulent mixing with coefficient $D_T = 10^8$–$5 \cdot 10^8$ cm^2 sec^{-1}, which carries CO_2 from the lower layers and CO and O to them. On the Earth, under similar conditions, the experiments give $D_T \approx 10^6$–10^7

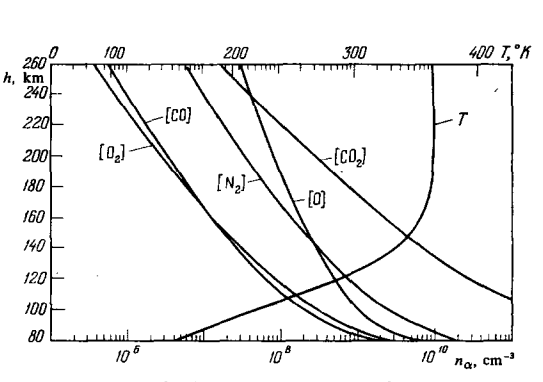

FIG. 23. Model of the composition of the upper atmosphere of Mars.

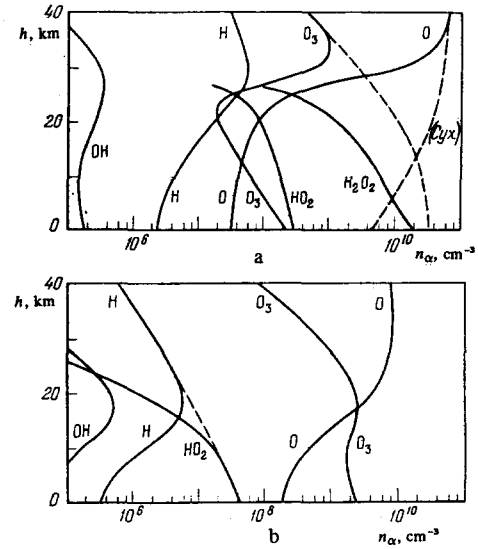

FIG. 24. Concentrations of the components in the atmosphere of Mars from the models of Parkinson and Hunten (a) and McElroy and Donahue (b).

cm^2 sec^{-1} at 100–110 km.

In[199] it was assumed that such transport is realized by large-scale winds, which were taken from the model of[194]. However, according to the model of[195], the global thermospheric circulation is closed already at altitudes of 115–130 km, from which it follows that mass motions do not remove the components to lower layers of the atmosphere.

Allowance for only the transport of CO and O to the lower layers of the atmosphere does not solve the problem of its composition: One must explain how CO and O are combined to CO_2 despite the fact that the reactions (22) and (23) are much slower than the O + O recombination reaction (24). To explain the predomiance of CO_2 under these conditions, the reactions (36)–(48) were proposed; in them, components containing hydrogen (and on Venus chlorine also) catalyze the association of CO and O. With allowance for these reactions and also others associated with them (40–50 reactions altogether) models were calculated of the composition of the atmosphere of Mars[174,175,177] and the atmosphere of Venus above the clouds.[172,173,176,178,179] There are important differences between these models, reflecting the indeterminacy in the knowledge about the composition; moreover, it is not only the concentrations of the components that differ but also sometimes the nature of the vertical profile; for example, in Fig. 24 one can see that there is an important difference between the profiles of the ozone concentration on Mars according to the models of[174,175]. The experiments on Mars 6 ([200]) gave a profile closer to that of the model of[174].

For Mars, even with allowance for these chemical reactions, which are effective in the lower atmosphere, good agreement with the experiments for the concentrations in the thermosphere were obtained with a high value of the coefficient of turbulent mixing: $D_T = 1.5 \cdot 10^8$ cm^2 sec^{-1}.[175]

Models of the atmosphere of Venus above the clouds[175,179] show that if the oxygen concentration at 140 km is $n_0(140) \approx 1\%$ then $D_T \approx 10^7$ cm^2 sec^{-1} is sufficient and if $n_0(140) \approx 10\%$, then even $D_T \approx 10^6$ cm^2 sec^{-1} is sufficient. However, the need to reconcile the data on the components containing hydrogen with the data on the dissociation of hydrogen (see Sec. E in Ch. 5) leads to values $D_T \approx 5 \cdot 10^7$ cm^2 sec^{-1}, though this value can be reduced if one allows the occurrence of additional nonthermal dissociation.[178,179] Figure 25 shows a variant of the model of the composition of the upper atmosphere of Venus calculated for $D_T = 6 \cdot 10^6$ cm^2 sec^{-1}.[179]

The above shows that the picture of the composition of the upper atmospheres of Mars and Venus and the processes governing it still contains serious obscurities. To make the picture more accurate, we need measurements of the concentrations of a number of components, laboratory measurements of the coefficients of various reactions and calculations of more detailed models; measurements of the intensity of turbulent mixing would be of decisive importance.

D. Models of the ionosphere

The profiles of the electron density in the dayside ionosphere of Mars and Venus up to altitudes of several tens of kilometers above the n_e maximum were calculated in[51,52,79,184–187,201] under the condition of photochemical equilibrium: Since diffusion can be ignored here, it was assumed that the number of electron–ion pairs generated in 1 cm^3 in one second by photoionization is equal to the number that disappear as a result of recombina-

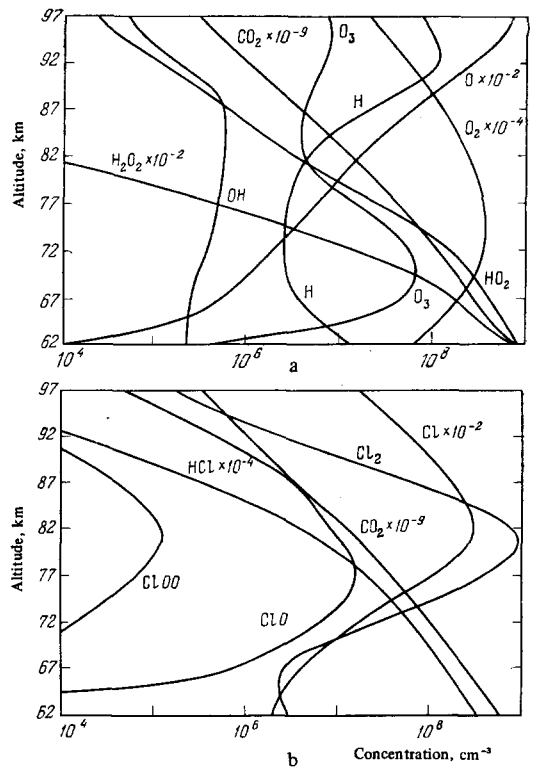

FIG. 25. Model of composition of the upper atmosphere of Venus.

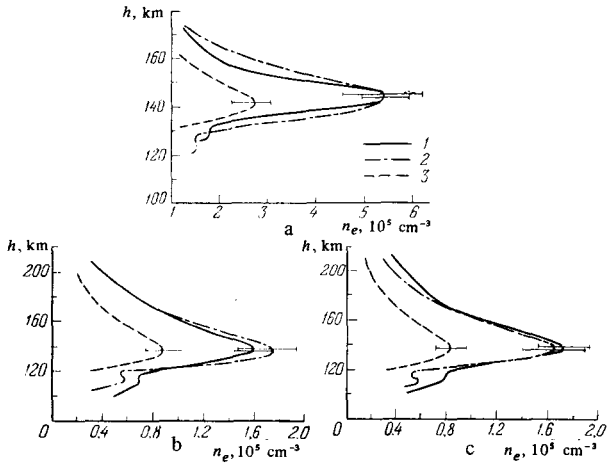

FIG. 26. Profiles of the electron density onVenus from measurements by Mariner 5 (a) and on Mars from measurements by Mariner 6 (b) and Mariner 7 (c). 1) Experiment, 2) calculation from experimental flux $F_{\lambda\infty}$, 3) calculation from $4F_{\lambda\infty}$.

tion, $P_{(e,i)} = L_{(e,i)}$, which with allowance for the predominance of CO_2 and the presence in the ionosphere of CO_2^+ and O_2^+ ions can be written in the following form (the notation is the same as in Eq. (13)):

$$n_{CO_2} \int_0^{\lambda_{max}} \frac{F_{\lambda\infty}}{h\nu} \sigma_{CO_2}^{ion}(\lambda) \exp(-n_{CO_2} H_{CO_2} \sigma_{CO_2})\, d\lambda = n_e(\alpha_1 n_{CO_2^+} + \alpha_2 n_{O_2^+}). \quad (52)$$

Without the ion composition being made more precise, the right-hand side, with allowance for quasineutrality ($n_e = n_+$), was usually replaced by

$$L_{(e,i)} = \alpha_{eff} n_e^2. \quad (53)$$

As was noted in[96], it follows from (52) and (53) that where the CO_2 layer is optically thin and there is photochemical equilibrium the scale height of the electrons is determined by the formula $H_e = 2R_0T/M_{CO_2}g$ and not by $H_e = 2R_0T_p/\bar{M}_+ g$ ($T_p = (T_e + T_i)/2$), $\bar{M}_+$ is the mean molecular weight of the ions), as would be the case in diffusion equilibrium, which simplifies the determination of T from H_e.

The $n_e(h)$ profiles (Fig. 26) calculated in this way in the models of[51,52] agree in their general features with the experimental profiles; one can see not only the principal maximum but also an indent somewhat below it, and it can be seen from the calculation that the main layer is formed as a result of photoionization of CO_2 by ultraviolet solar radiation and the indent by photoionization by soft x-rays. Therefore, the main layer can be regarded as analogous to the F_1 layer of the terrestrial ionosphere and the indent as a analogous to the E layer.

In the models of[184,187], which gave good agreement between the $n_e(h)$ profiles and the experimental profiles for Venus, the scale height for the electrons H_e above the n_e maximum on Mars was found to be much too large; the reason for this was the overestimation of T_∞ due to overestimation of ε.

In general, there is satisfactory agreement between the calculated and experimental $n_e(h)$ profiles but there is an important difference: In the calculation the electron density at the maximum of the layer, $n_{e,max}$, is 1.5–2 times less than according to the experiments (see Fig. 26). It follows from this, with allowance for (52) and (53), that to reconcile the calculated $n_{e,max}$ with the experimental values it is either necessary to increase by 3–4 times the flux $F_{\lambda\infty}$ (reducing by as many times ε in order not to obtain improbably large values of T_∞) or to decrease by as many times α ([61]) or to assume that an additional ionization source is provided by interaction of protons of the solar wind with atmospheric particles.[52] To establish the real mechanism, we need further investigations of all these parameters.

Comparison of the experimental and calculated profiles gives indirect but convincing information about the neutral composition: The best agreement of these profiles is obtained with an atmosphere of pure CO_2, and an assumption of 10% dissociation of CO_2—or addition of 10% nitrogen or 1% molecular oxygen—only increases the difference between the calculated and experimental profiles.[51]

According to calculations made under certain assumptions about the chemical reactions,[202,203] there is on Mars also an analog of the terrestrial D layer—a region below about 20–25 km, extending to the surface of the planet, where the concentration of electrons and negative ions is about 10^2–10^3 cm^{-3}.

To determine the ion composition on Mars and Venus, it is necessary to remember that the fast ion–molecule reactions (28)–(31) transform CO_2^+ into O_2^+. Since the O_2^+ ions are formed mainly in these reactions (the source due to direct photoionization of O_2 is negligibly small because of the low concentration of molecular oxygen) and disappear in the dissociative recombination reaction (35), we obtain from the equilibrium condition

$$\frac{n_{O_2^+}}{n_{CO_2^+}} = \frac{(k_{28} + k_{29}) n_O}{\alpha_{O_2^+} n_e}. \quad (54)$$

Substitution of the experimental values of n_O and n_e leads to a predominance of O_2^+ (Fig. 27).[72]

An increase of the scale height of the electrons at large altitudes (see Fig. 5) indicates that here a light ion (or light ions) predominate: H^+, H_2^+, or He^+.[204–207] The ion distribution on Venus calculated under the last assumption is shown in Fig. 28, which is taken from[207].

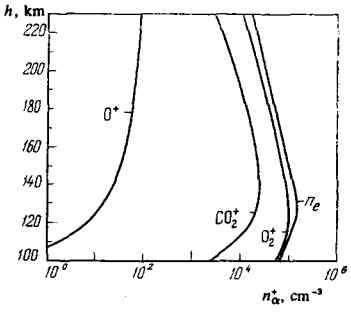

FIG. 27. Model of the ion composition of the ionosphere of Mars.

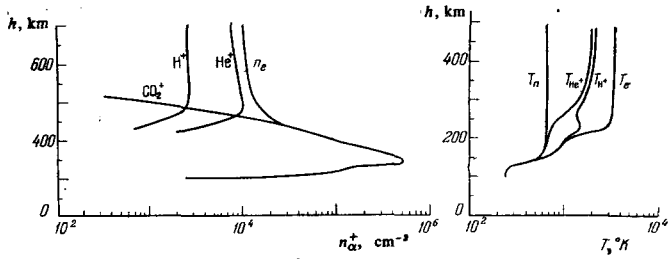

FIG. 28. Ion composition of the upper ionosphere of Venus (a) and the temperatures T_e, T_i, T_n (b).

In[208], the $n_e(h)$ profile on Venus measured by Mariner 10 at a time of low solar activity was satisfactorily described under the assumption that at $h \approx 180-240$ km O^+ ions predominated and at greater altitudes He^+, while at lower altitudes O_2^+ and CO_2^+.

In calculating the ion composition on Venus, Kumar and Hunten[209] assumed $T_\infty = 350$ °K for high solar activity (interpreting the hydrogen profile $n_H(h)$ measured on Mariner 5 in the framework of a two-temperature model and assuming that the smaller scale height corresponds to the thermalized particles and the larger to superthermal particles); however, the agreement between the calculated $n_e(h)$ profile and the experimental profile in the region of the ionospheric maximum was not as good as in models in which $T_\infty = 700$ °K was assumed.

Calculations were made of the thermal regime of the ionospheres of Venus and Mars and the distributions of the electron and ion temperatures by integrating one-dimensional energy balance equations for the electrons and ions without allowance for the influence of motions and under a number of other simplifications; in particular, with simplified allowance for the transfer of energy from the photoelectrons to the electron gas.[159,207,210] The general picture of the $T_e(h)$ and $T_i(h)$ profiles obtained in these calculations is similar to the picture in the terrestrial ionosphere: Above a certain level, T_e appreciably exceeds the neutral temperature T, and the ion temperature T_i at low altitudes is closer to T, while at large altitudes it approaches T_e (see Fig. 28). However, some details of this picture are different in different models: According to[159,210], the difference between T_e, T_i and T is negligibly small right up to 180–200 km, whereas according to[207] T_e appreciably exceeds T already at 200 km.

Estimates made for the nightside ionosphere on Venus showed that the light ions can be carried by wind from the day to the night side (since the ions are readily carried along by the neutrals in the weak magnetic field of the planet), and the ions transported thus then diffuse downward, as a result of which there is established a diffusion–equilibrium profile of the light ions, and the lower part of the nightside ionosphere (at $h \lesssim 200$ km), where the small scale height indicates the presence of a heavy ion, may arise from the charge exchange reaction of the light ions in CO_2.[211]

Thus, for a better description of the ionospheres, we need to know more accurately the rate of ion production (for which it is necessary to obtain more accurately the spectral flux of the solar radiation at different levels of the solar activity), and also the rate of recombination of the ions with allowance for the presence of excited particles. It is necessary to determine more precisely the ion composition, including the light ions, take into account the dynamical factors influencing the distribution of the electrons and ions, and investigate the mechanisms of formation of the nightside ionosphere. It is also necessary to investigate the influence of the solar wind on the ionosphere.

E. Exosphere and dissipation of gases from the atmosphere

In the exosphere, where the mean free path of the particles is greater than the scale height, the atoms and molecules move virtually without collisions. Those of them that in their last collision near the thermopause acquired a velocity less than the escape velocity move along ballistic trajectories and are returned to the thermosphere (the ballistic component); a certain number move in elliptical orbits that lie entirely in the exosphere (the satellite component); finally, those that in their last collision acquired a velocity greater than the escape velocity from molecules in the high-energy tail of the Maxwell distribution diffuse out of the atmosphere (the evaporating component).[212–215] Only the light components can leave the atmosphere in appreciable numbers by thermal dissipation, though there are also nonthermal mechanisms of dissipation.[81,178,179]

Allowance for dissipation of the gases is important both in the study of the contemporary composition and in the study of the evolution of planetary atmospheres. The flux of particles of component k which leave the atmosphere as a result of thermal dissipation can be expressed by Jeans's formula, which is obtained by integrating the Maxwellian velocity distribution over the greater than critical velocities:

$$\Phi_k = n_c \frac{v_T}{2\sqrt{\pi}} (1+\xi_c)\, e^{-\xi_c}, \qquad (55)$$

where $v_T = \sqrt{2k/Tm}$ is the most probable thermal velocity, $\xi = GmM/krT = v_{esc}^2/v_T^2 = r/H$, where v_{esc} is the escape velocity, G is the gravitational constant, r is the planetocentric radius, m is the mass of the molecule, M is the mass of the planet; the index c designates the conditions at the base of the exosphere, where $l = H$.

The assumptions under which Eq. (55) were obtained are that there is a sharp boundary at altitude h_c between the thermosphere and the exosphere; that at it the Maxwellian distribution persists; and that immediately above it the molecules move without collisions. These simplify the real picture. However, calculations of the transition layer between the terrestrial thermosphere and exosphere (by the Monte Carlo method) have shown that refinements lead only to a small correction to Jeans's formula: the evaporating hydrogen flux (from a medium of atomic oxygen) is reduced by 20–25% compared with this formula, and the helium flux is reduced by 3–5%.[213,214]

Although the evaporating flux in Eq. (55) is expressed

in terms of the characteristics at the base of the exosphere, h_c, its magnitude is sometimes determined by the physical conditions at a lower level h_d near the homopause. This occurs if the diffusion velocity of the evaporating component at this level, w_d, is less than the escape velocity at the critical level $w_c (w_d \approx D_k/H_m$, D_k is the diffusion coefficient of the evaporating component and H_m is the scale height of the main component).[215] It follows from this that a complete description of the dissipation process is possible only in the framework of a complete model of the composition, i.e., by solving the system of the continuity equations for the components with allowance for molecular diffusion, turbulent mixing, and chemical reactions, and also with allowance for the evaporating fluxes in the upper boundary c conditions.

On Mars, the height of the base of the exosphere lies, according to the different estimates, in the range $h_c = 180-230$ km (which may partily reflect real variations of the height). The evaporating flux of hydrogen atoms calculated in accordance with measurements of the scattered radiation in Lyman α (1216 Å) by Mariner 6, 7, and 9 is $\Phi_H \approx (1.8-2.0) \cdot 10^8$ cm^{-2} sec^{-1}.[8,74] This value agrees ssatisfactorily with the flux obtained in models of the composition in which the atomic hydrogen is produced mainly as a result of photodissociation of water and in some subsequent reactions and then diffuses into the exosphere, the evaporating flux being determined by the diffusion flux; in these models $\Phi_H \approx (1.0-1.2) \cdot 10^8$ cm^{-2} sec^{-1}.[215,216]

On Venus, the base of the exosphere lies at approximately $h_c \approx 210-250$ km. The evaporating flux of hydrogen atoms calculated from measurements of the line 1216 Å by Mariner 5 is $\Phi_H \approx 10^6$ cm^{-2} sec^{-1}.[217,218] At the same time, the value of this flux calculated from the concentration of H_2O, HCl, and H_2 at the upper boundary of the clouds is about 100 times greater, i.e., $\Phi_H \geq 10^8$ cm^{-2} sec^{-1}.[215] To explain this discrepancy, it is necessary to assume either a large coefficient of turbulent mixing, $D_T \geq 5 \cdot 10^7$ cm^{-2} sec^{-1} (which, incidentally, reduces the oxygen concentration) or that there is additional nonthermal dissociation of hydrogen.[178,179]

Additional nonthermal dissipation is possible by the following mechanisms. On Mars, because of the comparatively weak gravitational field the escape energies are low (for CO, C, N, O, H they are respectively, 3.49, 1.49, 1.74, 1.99, 0.12 eV); in some of the reactions that take place in the exosphere the reaction products can obtain from internal energy a kinetic energy greater than the escape energy and leave the atmosphere.[81,177] This can happen, for example, in the case of dissociative recombination: $CO_2^+ + e \rightarrow CO + O$; $O_2^+ + e \rightarrow O + O$. According to the estimates of McElroy,[81] the evaporating flux of oxygen atoms due to this process is $\Phi_0 = (6-8) \cdot 10^7$ cm^{-2} sec^{-1}, i.e., it is about half the flux of the hydrogen atoms and thus can ensure the escape of oxygen atoms formed by the photodissociation of water.

On Venus, charge exchange and dissociative recombination reactions can produce hydrogen atoms with high velocities that escape from the atmosphere.[179] In addition, on Mars and Venus both light and heavy ions can be "swept" out of the upper ionosphere by the plasma flux of the solar wind (see Sec. F of Ch. 5).

F. Influence of solar wind on the atmosphere

On Mars and Venus, the solar wind (the flux of solar plasma) has a very important influence on the atmosphere because of the weak magnetic fields of these planets. According to the measurements, the magnetic fields of Mars and Venus are about 10^{-4} of the terrestrial magnetic field; Mars apparently has an intrinsic magnetic moment while the magnetic field of Venus is probably induced by the effect of the solar wind on the ionosphere.[219-224]

The nature of the influence has not yet been completely clarified, though the main features are as follows.[225-230] The plasma of the solar wind (with concentrations of a few particles per 1 cm^3, frozen magnetic field $\overline{B}_{sw} \approx 5-20$ γ, and velocities of about 300–600 km/sec near Venus and Mars) compresses the ionospheric plasma on the dayside, forming a sharp boundary—the plasmopause or ionopause—while on the nightside it forms the tail of the plasmosphere; the streamlines of the solar wind are deflected, so that it flows round the plasmosphere. Above and along the flux a shock wave is formed, in which the velocity, magnetic field, and temperature of the solar wind change abruptly.

The plasmopause on Venus was discovered at an altitude of about 500 km by means of the radar-occultation experiments with Mariner 5 (see Fig. 5). The presence of a shock wave near Mars and Venus has been confirmed by magnetic and plasma measurements by Venera 4 and 6, Mariner 4 and 5, and Mars 2 and 3.[231-238] The shape of the shock wave agrees satisfactorily with the one calculated in the framework of the hypersonic gas-dynamic model.[223-227]

The position of the plasmopause is determined in the hydrodynamic approximation by the condition of balance of the dynamic pressure of the solar wind and the pressure of the ionosphere:

$$\varkappa n_{sw} m_{sw} v_{sw}^2 \cos^2(\xi) + \frac{\overline{B}_{sw}^2}{8\pi} = k(n_e T_e + n_i T_i) + \frac{\overline{B}^2}{8\pi}, \qquad (56)$$

where n_{sw}, m_{sw}, v_{sw}, $\overline{B}_{sw}$ are the concentration, the mass of the particles, the velocity, and the magnetic field in the solar wind, $\varkappa \approx 0.88$ for the flow considered here; n_e, n_i, T_e, T_i are the concentrations and temperatures of the ionospheric electrons and ions, and $\overline{B}$ is the magnetic field in the ionosphere; ξ is the angle between the outer normal to the mesopause and the velocity of the unperturbed solar wind.

Note that neglect of the interaction between the solar wind and the neutral particles simplifies the real picture since although the cross sections of interaction of solar-wind particles with the neutral particles are smaller than those with the charged particles, there are many more neutral than charged particles near the base of the exosphere.

From Eq. (56) and using the experimental data on the height of the plasmopause on Venus and parameters of the ionosphere and the solar wind it was found that the magnetic field on Venus at altitude 500 km is $\overline{B} \approx 20$–$30\ \gamma$.[207]

Cloutier and Daniell,[228] specifying a model of the ionosphere and calculating the altitude distribution of the conductivity and the currents induced by the solar wind and their magnetic field, found the magnetopause as the altitude at which the induced magnetic field becomes equal to the magnetic field of the solar wind: They obtained a plasmopause at about 500 km on Venus and 350–425 km on Mars (without allowance for its intrinsic magnetic moment). On the basis of this model, it was then calculated[229] that the influence of the particles of the solar wind on the ionospheric particles above the plasmopause leads to the latter being "swept out" of the atmosphere, and although these losses are small (8 g/sec on Mars and 12 g/sec on Venus), the profiles of the ionospheric ions and electrons above the plasmopause are strongly distorted from the barometric distributions.

Bauer and Hartle[230] who assumed on the basis of[224] that Mars has an intrinsic magnetic moment $M \approx 2.4 \cdot 10^{22}$ G/cm^3 (magnetic field on the surface $\overline{B}_0 \approx 60\ \gamma$), found by approximate estimates that the magnetopause in the subsolar point is at the altitude 990 km (where $\overline{B} \approx 20\ \gamma$) and that at about 300 km there is a plasmopause, below which the ionospheric plasma is in hydrostatic equilibrium and rotates with the planet and above which there are large-scale convective currents of thermalized plasma induced by the solar wind.

The possibility that particles of the solar wind penetrate into the plasmosphere has not yet been sufficiently studied. It has been shown[9] that the hydrodynamic relation (5.6), which essentially determines the plasmopause as a wall that is inpenetrable for particles of the solar wind, is approximate; in reality, turbulence of the plasma behind the shock wave may cause instabilities to arise on the plasmopause, and these can allow particles of the solar wind to enter the plasmosphere. On the basis of these ideas, an energy source was introduced in some ionospheric models at the upper boundary of the ionosphere.[206,207,210] On the other hand, in[229], also on the basis of a qualitative argument, it was found that if particles of the solar wind pass through the plasmopause electric forces arise which prevent their penetration into the plasmosphere and return them to the outer flux. In the model of[229] there is a sink on the upper boundary of the ionosphere due to the ionospheric particles being "swept out" by the solar wind.

A further study of the interaction of the solar wind with the atmosphere is needed in order to make more precise the upper boundary conditions in theoretical models of the atmosphere and the ionosphere.

6. CONCLUSIONS

The results of experiments made in recent years by means of space probes in conjunction with the data of terrestrial observations have provided information about a number of the structural parameters of the upper atmospheres—the temperatures, density, composition, and electron density. These data and general physical laws have been used to calculate models which, under certain simplifications, describe the picture of spatial distributions and time variations of the structural parameters and also establish the main factors and mechanisms which determine this picture. These models were then used to interpret the experimental data. But the picture is far from complete and it contains a number of obscurities and contradictions; in addition, new problems arise that need solutions.

In order to determine the composition more accurately and explain the predominance of CO_2 up to high altitudes the following are required: more accurate measurements of the concentrations of the main components of the atmosphere and also the concentrations or total content of a number of small components such as H_2, H, N_2, O_2, H_2O, O_3, Ar; investigation of the intensity of turbulent mixing and the altitude of the turbopause; laboratory investigations of the rates of a number of reactions, including reactions with the participation of excited particles.

To determine more precisely the thermal regime and the distribution and variations of the temperature we need: more accurate measurements of the spectral flux of solar radiation at different levels of solar activity; clarification of the contribution of additional heat sources, in particular, dissipation of atmospheric gravity waves that arrive from the lower atmosphere; calculations of the heating efficiency resulting from the absorption of ultraviolet photons.

To get a more accurate description of the ionospheres, we need to know more accurately the rates of ion production and recombination of ions, to take into account the influence of dynamical factors, especially on the structure of the nightside ionosphere, and to investigate the influence of solar wind.

To make more precise the interpretation of experimental data obtained by measurement of atmospheric emissions we need investigations of the relative importance of the different processes of excitation of atmospheric particles.

For a complete and detailed description of the structure and dynamics of the planetary upper atmospheres an important role may be played by calculations of three-dimensional nonstationary models describing the coupling of the thermal regime, the composition, and the dynamics of the upper atmospheres.

Note added in proof. On October 22 and 25, 1975, the space probes Venera 9 and 10 were put into orbits around Venus, and landers separated from them made a soft landing and transmitted pictures of the surface of the planet at the touchdown position. Besides investigations of the surface and troposphere, investigations were also made of the upper atmosphere of Venus.[253] Measurements with an ultraviolet photometer of the scattered radiation in the line 1216 Å makes it possible to find the distribution of the hydrogen concentration and

the temperature of the exosphere. A spectrometer measured the emission spectrum of the nightside atmosphere in the range 3000–8000 Å, which will help to clarify the processes taking place in the atmosphere. The profiles of the electron density in the ionosphere and the profiles of the neutral concentration and the temperature in the mesosphere were obtained by radar-occultation. An infrared radiometer measured the temperature of the upper boundary of the clouds (about 233 °K on the dayside and 11–12° higher on the nightside). In addition, data were obtained on the magnetic field in the neighborhood of Venus and the manner in which the solar wind flows round the planet, these confirming the data obtained earlier. The results of the measurements are currently being evaluated.

[1]V. I. Moroz, Usp. Fiz. Nauk **104**, 255 (1971) [Sov. Phys. Usp. **14**, 317 (1971)].
[2]M. Ya. Marov, Icarus **16**, 415 (1972).
[3]A. D. Kuz'min and M. Ya. Marov, Fizika Planety Venera (Physics of the Planet Venus), Nauka, Moscow (1974).
[4]V. A. Konashenok and K. Ya. Kondrat'ev, Novoe o Venere i Marse (New Results on Venus and Mars), Gidrometeoizdat, Leningrad (1970).
[5]K. Ya. Kondrat'ev and A. M. Bunyakova, Meteorologiya Marsa (Meterology of Mars), Gidrometeoizdat, Leningrad (1973).
[6]J. C. McConnell, in: Physics and Chemistry of Upper Atmospheres, D. Reidel, Dordrecht-Boston (1973), p. 309.
[7]R. G. Prinn, in: Physics and Chemistry of Upper Atmospheres, D. Reidel, Dordrecht-Boston (1973), p. 353.
[8]C. A. Barth, Ann. Rev. Earth and Planet. Sci. **11** (1974).
[9]R. C. Whitten and L. Colin, Rev. Geophys. and Space Phys. **12**, 155 (1974).
[10]V. I. Moroz, Fizika Planet (Physics of the Planets), Nauka, Moscow (1967).
[11]R. E. Dickinson, J. Atmos. Sci. **29**, 1531 (1972).
[12]A. P. Vinogradov *et al.*, Dokl. Akad. Nauk SSSR **179**, 37 (1968) [Sov. Phys. Dokl. **13**, 176 (1968)].
[13]A. P. Vinogradov, Yu. A. Surkov, and V. M. Andreichikov, Dokl. Akad. Nauk SSSR **190**, 552 (1970) [Sov. Phys. Dokl. **15**, 4 (1970)].
[14]V. S. Avduevskiĭ *et al.*, Dokl. Akad. Nauk SSSR **179**, 310 (1968) [Sov. Phys. Dokl. **13**, 186 (1968)].
[15]V. S. Avduevskiĭ, M. Ya. Marov, and M. K. Rozhdestvenskii, Kosmich. Issled. **7**, 233 (1969).
[16]V. S. Avduevsky *et al.*, J. Atmos. Sci. **28**, 263 (1971).
[17]M. Ya. Marov *et al.*, J. Atmos. Sci. **30**, 1210 (1973).
[18]A. Kliore and D. L. Cain, J. Atmos. Sci. **25**, 549 (1968).
[19]A. Kliroe *et al.*, in: Space Research, Vol. 9, North-Holland, Amsterdam (1969), p. 712.
[20]G. Fjeldbo, A. Kliore, *et al.*, Astron. J. **76**, 123 (1971).
[21]R. Eshleman, Radio Sci. **5**, 325 (1970).
[22]S. I. Rasool and R. W. Stewart, J. Atmos. Sci. **28**, 869 (1971).
[23]H. T. Howard *et al.*, Science **183**, 1297 (1974).
[24]G. de Vaucouleurs and D. H. Menzel, Nature **188**, 28 (1960).
[25]G. de Vaucouleurs, Icarus **3**, 187 (1964).
[26]V. G. Kurt, S. B. Dostovalow, and E. K. Sheffer, J. Atmos. Sci. **25**, 668 (1968).
[27]V. G. Kurt and A. S. Smirnov, in: Space Research, Vol. 11, Akademie-Verlag, Berlin (1971), p. 134.
[28]C. A. Barth, J. Atm. Sci. **25**, 564 (1968).
[29]C. Barth *et al.*, Science **158**, 1678 (1967).
[30]C. A. Barth *et al.*, J. Geophys. Res. **73**, 2541 (1968).
[31]C. A. Barth, in: Planetary Atmospheres (ed. C. Sagan, T. Owen, and H. Smith), D. Reidel, Dordrecht (1971), p. 17.
[32]L. Wallace, J. Geophys. Res. **74**, 115 (1969).
[33]T. M. Donahue, J. Geophys. Res. **74**, 1128 (1969).
[34]T. M. Donahue, J. Atmos. Sci. **25**, 568 (1968).
[35]T. M. Donahue, J. Atmos. Sci. **28**, 895 (1971).
[36]A. L. Broadfoot *et al.*, Science **183**, 1315 (1974).
[37]M. B. McElroy and J. C. McConnell, J. Atmos. Sci. **28**, 879 (1971).
[38]G. E. Thomas, J. Atmos. Sci. **28**, 859 (1971).
[39]D. J. Strickland *et al.*, J. Geophys. Res. **77**, 4052 (1972); **78**, 4547 (1973).
[40]D. J. Strickland, J. Geophys. Res. **78**, 2827 (1973).
[41]H. W. Moos *et al.*, Astrophys. J. **155**, 887 (1969).
[42]H. W. Moos and G. J. Rottman, Astrophys. J. **169**, L127 (1971).
[43]G. J. Rottman and H. W. Moos, J. Geophys. Res. **78**, 8033 (1973).
[44]H. W. Moos, J. Geophys. Res. **79**, 685 (1974).
[45]P. M. Woiceshyn, Icarus **22**, 325 (1974).
[46]K. I. Gringauz and T. K. Breus, Kosmich. Issled. **7**, 871 (1969).
[47]J. Pirraglia and S. H. Gross, Planet. and Space Sci. **18**, 1769 (1970).
[48]P. T. McCormick and R. C. Whitten, Planet. and Space Sci. **20**, 822 (1972).
[49]G. Fjeldbo *et al.*, J. Geophys. Res. **70**, 3701 (1965).
[50]G. Fjeldbo and V. R. Eshleman, Radio Sci. **4**, 879 (1969).
[51]R. W. Stewart, J. Atmos. Sci. **25**, 578 (1968).
[52]R. W. Stewart, J. Atmos. Sci. **28**, 1069 (1971).
[53]C. Boyer and H. Camichel, Ann. Astrophys. **24**, 531 (1961).
[54]C. Boyer, Planet. and Space Sci. **21**, 1559 (1973).
[55]B. A. Smith, Science **158**, 114 (1967).
[56]A. Dolfus, in: Atmospheres of Venus and Mars, Gordon and Breach, New York (1968), p. 147.
[57]B. C. Murray *et al.*, Science **183**, 1307 (1974).
[58]T. Gold and S. Soter, Icarus **14**, 16 (1971).
[59]R. Thompson, J. Atmos. Sci. **27**, 1107 (1970).
[60]R. E. Young and G. Shubert, Planet. and Space Sci. **21**, 1563 (1973).
[61]C. B. Leovy, J. Atmos. Sci. **30**, 1218 (1973).
[62]V. G. Istomin *et al.*, Kosmich. Issled, **13**, 16 (1975).
[63]C. B. Leovy and Y. Mintz, J. Atmos. Sci. **26**, 1167 (1969).
[64]G. S. Golitsyn, Vvedenie v Dinamiku Planetnykh Atmosfer (Introduction to the Dynamics of Planetary Atmospheres), Gidrometeoizdat (1973).
[65]N. N. Dementjeva *et al.*, Icarus **17**, 475 (1972).
[66]V. G. Kurt *et al.*, Kosmich. Issled. **11**, 315 (1973).
[67]V. G. Kurt *et al.*, Icarus **21**, 35 (1974).
[68]J. L. Bertaud *et al.*, Kosmich. Issled. **13**, 42 (1975).
[69]S. B. Dostovalov and S. D. Chuvakhin, Kosmich, Issled. **11**, 767 (1973).
[70]C. A. Barth *et al.*, Science **165**, 1004 (1969).
[71]C. A. Barth *et al.*, J. Geophys. Res. **76**, 2213 (1971).
[72]C. A. Barth *et al.*, Science **175**, 309 (1972).
[73]C. A. Barth *et al.*, Icarus **17**, 457 (1972).
[74]A. I. Stewart *et al.*, Icarus **17**, 469 (1972).
[75]D. E. Anderson and C. W. Hord, J. Geophys. Res. **76**, 6666 (1971).
[76]E. S. Barker *et al.*, Science **170**, 1308 (1970).
[77]V. I. Moroz and L. É. Nadzhip, Kosmich. Issled. **13**, 33 (1975).
[78]J. C. McConnell and M. B. McElroy, J. Geophys. Res. **75**, 7290 (1970).
[79]M. B. McElroy and J. C. McConnell, J. Geophys. Res. **75**, 6674 (1971).
[80]A. Dalgarno and M. B. McElroy, Science **170**, 167 (1970).
[81]M. B. McElroy, Science **175**, 443 (1972).
[82]A. I. Stewart, J. Geophys. Res. **77**, 54 (1972).
[83]V. A. Krasnopolsky, Icarus **24**, 28 (1975).
[84]A. Kliore *et al.*, Science **149**, 1243 (1965).
[85]G. Fjeldbo and V. R. Eshleman, Planet. and Space Sci. **16**, 1035 (1968).
[86]A. Kliore *et al.*, Science **166**, 1393 (1969).

[87]G. A. Fjeldbo *et al.*, Radio Sci. **5**, 381 (1970).
[88]A. J. Kliore *et al.*, Science **175**, 313 (1972).
[89]A. J. Kliore *et al.*, J. Geophys. Res. **78**, 4331 (1973).
[90]A. J. Kliore *et al.*, Icarus **17**, 484 (1972).
[91]M. A. Kolosov *et al.*, Radiotekh. Elektron. **17**, 2483 (1972).
[92]M. A. Kolosov *et al.*, Radiotekh. Elektron. **18**, 2009 (1973).
[93]M. B. Vasil'ev *et al.*, Kosmich. Issled. **13**, 48 (1975).
[94]M. A. Kolosov *et al.*, Kosmich. Issled. **13**, 54 (1975).
[95]J. S. Hogan and R. W. Stewart, Radio Sci. **7**, 525 (1972).
[96]M. N. Izakov, Kosmich. Issled. **11**, 761 (1973).
[97]R. W. Stewart and J. S. Hogan, Science **165**, 386 (1969).
[98]S. Chapman, transl. in: Fizika Verkhnei Atmosfery (Physics of the Upper Atmosphere), Fizmatgiz, Moscow (1963), p. 13.
[99]M. Nicolet, transl. in., Aeronomiya (Aeronomy), Mir, Moscow (1964).
[100]A. I. Ivanovskiĭ, A. I. Repnev, and E. G. Shvidkovskiĭ, Kineticheskaya Teoriya Verkhnei Atmosfery (Kinetic Theory of the Upper Atmosphere), Gidrometeoizdat, Leningrad (1967).
[101]M. N. Izakov, Space Sci. Rev. **7**, 579 (1967).
[102]M. N. Izakov, Dokl. Akad. Nauk SSSR **177**, 1324 (1967).
[103]M. N. Izakov, Space Sci. Rev. **12**, 261 (1971).
[104]P. M. Banks and G. Kockarts, Aeronomy, Academic Press, New York (1973).
[105]N. W. Spencer, L. U. Brace *et al.*, J. Geophys. Res. **67**, 157 (1962).
[106]J. R. Herman, A Possibility of Multiple Thermospheric Temperatures for Venus and Mars. Report at IAGA Assembly, Moscow (1971).
[107]J. C. G. Walker, cited in[6] on p. 203.
[108]A. D. Danilov and M. N. Vlasov, Fotokhimiya Ionizovannykh i Vozbuzhdennykh Chastits v Nizhneĭ Ionosfere (Photochemistry of Ionized and Excited Particles in the Lower Ionosphere), Gidrometeoizdat, Leningrad (1973).
[109]K. Ya. Kondrat'ev and V. A. Konashenok, in: Problemy Fiziki Atmosfery, Vol. 8 (Problems of The Physics of the Atmosphere), Izd-vo Leningr. Un-ta, (1970), p. 142.
[110]W. R. Kuhn and J. London, J. Atmos. Sci. **26**, 189 (1969).
[111]S. Chapman and T. G. Cowling, Mathematical Theory of Non-Uniform Gases, Cambridge (1952).
[112]J. O. Hirschfelder, C. F. Curtis, and R. B. Bird, Molecular Theory of Gases and Liquids, New York (1965).
[113]F. D. Colegrove *et al.*, J. Geophys. Res. **70**, 4931 (1965).
[114]F. D. Colegrove *et al.*, J. Geophys. Res. **71**, 2227 (1966).
[115]R. G. Roper, J. Geophys. Res. **71**, 5785 (1966).
[116]C. G. Justus, J. Geophys. Res. **72**, 1035 (1967).
[117]C. G. Justus and R. G. Roper, Meteorol. Monographs **8**, (No. 31), 122 (1968).
[118]F. S. Johnson and E. M. Wilkins, J. Geophys. Res. **70**, 1281, 4063 (1965).
[119]F. S. Johnson and B. Gottlieb, Planet. and Space Sci. **18**, 1707 (1970).
[120]D. M. Hunten, J. Geophys. Res. **79**, 1533 (1974).
[121]M. N. Izakov, Geomagn. Aeron. **10**, 283 (1970).
[122]S. Chapman, Proc. Phys. Soc. **43**, 483 (1931).
[123]J. W. Chamberlain and M. B. McElroy, Science **152**, 21 (1966).
[124]F. S. Johnson, transl. in: Okolozemnoe Kosmicheskoe Prostranstvo (Space in the Neighborhood of the Earth), Mir, Moscow (1966), p. 105.
[125]J. C. Brandt and P. W. Hodge, Solar System Astrophysics, New York (1964).
[126]H. E. Hinteregger, Ann. Geophys. **26**, 547 (1970).
[127]M. Ackerman, in: Mesopheric Models and Related Experiments, D. Reidel, Dordrecht (1971), p. 149.
[128]E. V. P. Smith and D. M. Gottlieb, Space Sci. Rev. **16**, 771 (1974).
[129]G. Schmidtke, Report at COSPAR Meeting, Varna (1975).
[130]G. S. Ivanov-Kholodnyi and V. V. Firsov, Geomagn. Aeron. **14**, 393 (1974).
[131]R. S. Nakata *et al.*, Sci. Light **14**, 54 (1965).
[132]M. J. Ogawa, J. Chem. Phys. **54**, 2550 (1971).
[133]G. R. Cook *et al.*, J. Chem. Phys. **54**, 2935 (1966).
[134]L. C. Lee *et al.*, J. Quantit. Spectr. and Rad. Transfer **13**, 1023 (1973).
[135]H. Sun and G. L. Weissler, J. Chem. Phys. **23**, 1625 (1955).
[136]E. C. Y. Inn and J. M. Heimerl, J. Atmos. Sci. **28**, 838 (1971).
[137]I. D. Clark and J. F. Noxon, J. Geophys. Res. **75**, 7303 (1970).
[138]C. D. Baulch and W. H. Breckenridge, Trans. Farad. Soc. **62**, 2768 (1966).
[139]T. G. Slanger and G. J. Black, J. Chem. Phys. **54**, 1889 (1971).
[140]B. H. Mahan, J. Chem. Phys. **33**, 959 (1960).
[141]G. M. Lawrence, J. Chem. Phys. **57**, 5616 (1972).
[142]G. M. Lawrence, J. Chem. Phys. **56**, 3435 (1972).
[143]D. L. Judge and L. C. Lee, J. Chem. Phys. **58**, 104 (1972).
[144]A. V. Dembovskii, M. N. Izakov, and O. G. Lisin, Kosmich. Isseld. **13**, 866 (1975).
[145]A. M. Pravilov and F. I. Vilesov, in: Uspekhi Fotoniki (Advances in Photonics), Izd-vo Leningr. UN-ta, (1973), p. 3.
[146]R. F. Heidner and D. Husain, Nature (Phys. Sci) **241**, 10 (1973).
[147]R. A. Young and G. Black, J. Chem. Phys. **44**, 3741 (1966).
[148]M. A. A. Clyne and B. A. Thrush, Proc. Roy. Soc. **A269**, 404 (1962).
[149]M. C. Lin and S. H. Bauer, J. Chem. Phys. **50**, 3377 (1969).
[150]T. G. Slanger and G. J. Black, J. Chem. Phys. **53**, 3722 (1970).
[151]H. I. Schiff, transl. in: Laboratornye Issledovaniya Aéronomicheskikh Reaktsiĭ (Laboratory Investigations of Aeronomical Reactions), Gidrometeoizdat, Leningrad (1970), p. 169.
[152]J. L. Bahr *et al.*, J. Quantit. Spectr. and Rad. Transfer **12**, 59 (1972).
[153]J. A. R. Samson and J. L. Gardner, J. Chem. Phys. **58**, 3771 (1973).
[154]J. A. R. Samson and J. L. Gardner, J. Geophys. Res. **78**, 3663 (1973).
[155]L. C. Lee and D. L. Judge, J. Chem. Phys. **57**, 4443 (1972).
[156]J. H. D. Eland, Intern. J. Mass Spectron. and Ion Phys. **9**, 397 (1972).
[157]J. Fryar and R. Browning, Planet. and Space Sci. **21**, 809, 1080 (1973).
[158]R. J. Van Brunt *et al.*, J. Chem. Phys. **57**, 3120 (1972).
[159]R. J. W. Henry and M. B. McElroy, cited in[26] on p. 251.
[160]T. Sawada *et al.*, J. Geophys. Res. **77**, 4812 (1972).
[161]M. Shimizu and O. Ashihara, Publ. Astron. Soc. Japan **24**, 201 (1972).
[162]F. C. Fehsenfeld *et al.*, J. Chem. Phys. **44**, 3022 (1966).
[163]F. C. Fehsenfeld *et al.*, J. Chem. Phys. **45**, 23 (1966).
[164]F. C. Fehsenfeld, D. B. Dunkin, *et al.*, Planet. and Space Sci. **18**, 1267 (1970).
[165]F. C. Fehsenfeld and E. E. Ferguson, J. Geophys. Res. **76**, 8453 (1971).
[166]F. C. Fehsenfeld *et al.*, J. Chem. Phys. **44**, 4087 (1966).
[167]M. A. Biondi, cited in[151] on p. 9.
[168]C. S. Weller and M. A. Biondi, Phys. Rev. Lett. **19**, 59 (1967).
[169]B. M. Smirnov, Iony i Vozbuzhdennye Atomy v Plazme (Ions and Excited Atoms in Plasmas), Atomizdat, Moscow (1974).
[170]E. C. Zipf, Bull. Amer. Phys. Soc. **15**, 418 (1970).
[171]R. A. Gutcheck and E. C. Zipf, J. Geophys. Res. **78**, 5429 (1973).
[172]R. G. Prinn, J. Atmos. Sci. **28**, 1058 (1971).
[173]R. G. Prinn, J. Atmos. Sci. **29**, 1004 (1972).
[174]T. D. Parkinson and D. M. Hunten, J. Atmos. Sci. **29**, 1380 (1972).
[175]M. B. McElroy and T. M. Donahue, Science **177**, 986 (1972).
[176]M. B. McElroy *et al.*, J. Atmos. Sci. **30**, 1437 (1973).

[177]D. M. Hunten, Rev. Geophys. Space Phys. 12, 529 (1974).
[178]S. C. Liu and T. M. Donahue, Icarus, 24, 148 (1975).
[179]N. D. Sze and M. B. McElroy, Planet. and Space Sci. 23, 763 (1975).
[180]F. Kaufmann, cited in[151] on p. 195.
[181]P. Connes *et al.*, Astrophys. J. 147, 1230 (1967).
[182]M. Schimizu, in: Space Research, Vol. 12, Akademie-Verlag, Berlin (1972), p. 293.
[183]M. B. McElroy, Astrophys. J. 150, 1125 (1967).
[184]M. B. McElroy, J. Geophys. Res. 73, 1513 (1968).
[185]M. B. McElroy, J. Atmos. Sci. 25, 574 (1968).
[186]M. B. McElroy, J. Geophys. Res. 74, 29 (1969).
[187]M. B. McElroy, Ann. Geophys. 26, 643 (1970).
[188]R. W. Stewart and J. S. Hogan, J. Atmos. Sci. 26, 330 (1969).
[189]M. N. Izakov and O. P. Krasitskiĭ, Geomagn. Aeron. 16, 209 (1976).
[190]F. S. Johnson, Science 150, 1445 (1965).
[191]M. Schimizu, Rept. Ionospher. and Space Res. Japan 20, 271 (1966).
[192]G. Fjeldbo *et al.*, J. Geophys. Res. 71, 2307 (1966).
[193]J. S. Hogan and R. W. Stewart, J. Atmos. Sci. 26, 332 (1969).
[194]R. E. Dickinson, J. Atmos. Sci. 28, 885 (1971).
[195]M. N. Izakov and S. K. Morozov, Kosmich. Issled. 13, 404 (1975).
[196]M. N. Izakov and S. K. Morozov, Kosmich. Issled. 14, 476 (1976).
[197]R. E. Dickinson, J. Atmos. Sci. 30, 296 (1973).
[198]T. Shimazaki and M. Shimizu, Rept. Ionospher. and Space Res. Japan 24, 80 (1970).
[199]R. E. Dickinson and E. C. Ridley, J. Atmos. Sci. 29, 1557 (1972).
[200]V. A. Krasnopol'skiĭ *et al.*, Kosmich. Issled. 13, 37 (1975).
[201]A. S. Vyshlov *et al.*, Kosmich. Issled. 13, 249 (1975).
[202]A. C. Aikin, Icarus 9, 487 (1968).
[203]R. C. Whitten *et al.*, Planet. and Space Sci. 19, 243 (1971).
[204]P. M. Banks, J. Geophys. Res. 76, 8455 (1971).
[205]P. M. Banks and W. I. Axford, Nature 225, 924 (1970).
[206]R. C. Whitten, J. Geophys. Res. 75, 3707 (1970).
[207]J. R. Herman *et al.*, Planet. and Space Sci. 19, 443 (1971).
[208]S. J. Bauer and R. E. Hartle, Geophys. Res. Lett. 1, 7 (1974).
[209]S. Kumar and D. M. Hunten, J. Geophys. Res. 79, 2529 (1974).
[210]R. C. Whitten, J. Geophys. Res. 74, 5623 (1969).
[211]M. B. McElroy and D. F. Strobel, J. Geophys. Res. 74, 1118 (1969).
[212]J. W. Chamberlain, Planet. and Space Sci. 11, 901 (1963).
[213]R. T. Brinkman, Planet. and Space Sci. 19, 791 (1971).
[214]J. W. Chamberlain and G. R. Smith, Planet. and Space Sci. 19, 675 (1971).
[215]D. M. Hunten, J. Atmos. Sci. 30, 1481 (1973).
[216]D. M. Hunten and M. B. McElroy, J. Geophys. Res. 75, 5989 (1970).
[217]M. B. McElroy and D. M. Hunten, J. Geophys. Res. 74, 1720 (1969).
[218]J. C. G. Walker *et al.*, J. Geophys. Res. 75, 3558 (1970).
[219]Sh. Sh. Dolginov *et al.*, Kosmich. Issled. 6, 561 (1968).
[220]Sh. Sh. Dolginov *et al.*, Kosmich. Issled. 7, 747 (1969).
[221]Sh. Sh. Dolginov *et al.*, in: Fizika Luny i Planet (Physics of the Moon and the Planets), Nauka, Moscow (1972), p. 283.
[222]H. S. Bridge *et al.*, Science 158, (3809), 1669 (1967).
[223]Sh. Sh. Dolginov *et al.*, Dokl. Akad. Nauk SSSR 207, 1296 (1972) [Sov. Phys. Dokl. 17, 1117 (1973)].
[224]Sh. Sh. Dolginov *et al.*, J. Geophys. Res. 78, 4779 (1973).
[225]A. J. Dessler, cited in[156] on p. 241.
[226]J. R. Spreiter and A. Y. Alksne, Ann. Rev. Fluid Mech. 2, 313 (1970).
[227]J. Spreiter *et al.*, Planet. and Space Sci. 18, 1281 (1970).
[228]P. A. Cloutier and R. E. Daniell, Planet. and Space Sci. 21, 463 (1973).
[229]P. A. Cloutier *et al.*, Planet. and Space Sci. 22, 967 (1974).
[230]S. J. Bauer and R. E. Hartle, J. Geophys. Res. 78, 3169 (1973).
[231]E. J. Smith *et al.*, Science 149, 1241 (1965).
[232]E. J. Smith, Adv. Astronaut. Sci. 25, 103 (1969).
[233]K. I. Gringauz *et al.*, Kosmich. Issled. 6, 411 (1968).
[234]K. I. Gringauz *et al.*, Kosmich. Issled. 8, 431 (1970).
[235]K. I. Gringauz *et al.*, Icarus 18, 54 (1973).
[236]O. L. Vaĭsberg *et al.*, Kosmich. Issled. 10, 462 (1972).
[237]O. L. Vaĭsberg *et al.*, Kosmich Issled. 11, 743 (1973).
[238]O. L. Vaĭsberg and A. V. Bogdanov, Kosmich. Issled. 12, 279 (1974).
[239]Ph. Sherman and L. Talbot, in: Gazodinamika Razrezbennykh Gazov (Russian translation of: Gas Dynamics of Rarefied Gases), IL. Moscow (1963), p. 266.
[240]R. W. Schunk, Planet. and Space Sci. 23, 437 (1975).
[241]L. Sirovich, in: Nekotorye Voposy Kineticheskoi Teorii Gazov (Russian translation of: Some Aspects of the Kinetic Theory of Gases), Mir, Moscow (1965), p. 186.
[242]H. Grad, Phys. Fluids 6, 147 (1963).
[243]D. A. Feier, in: Fizika Verkhnei Atmosfery Zemli (Physics of Upper Atmosphere of the Earth), Gidrometeoizdat, Leningrad (1971), p. 168.
[244]H. Rishbeth and O. K. Garriott, Introduction to Ionospheric Physics (1969).
[245]P. Banks, Planet. and Space Sci. 14, 1105 (1966).
[246]P. Stubbe, J. Atmos. and Terr. Phys. 30, 1965 (1968).
[247]S. -I. Akasofu and S. Chapman, Solar-Terrestrial Physics (1972).
[248]A. Dalgarno *et al.*, Planet. and Space. Sci. 15, 331 (1967).
[249]P. M. Banks, J. Geophys. Res. 72, 3365 (1967).
[250]J. R. Herman and S. Chandra, Planet. and Space Sci. 17, 815 (1969).
[251]E. Hesstvedt, in: Mesospheric Models and Related Experiments, D. Reidel, Dordrecht (1971), p. 52.
[252]F. S. Johnson, J. Atmos. Sci. 32, 1658 (1975).
[253]V. S. Avduevskii *et al.*, Pravda, February 21, 1976; O. L. Vaĭsberg *et al.*, Pis'ma Astron. Zh. 2, 3 (1976).

Translated by Julian B. Barbour